BM@N Analysis Note 3
Production of π^+, K^+ mesons in
3.2 A GeV argon-nucleus interactions

Analysis team: M.Kapishin, L.Kovachev, V.Plotnikov, Yu.Petukhov, I.Rufanov, M.Zavertyaev, A.Zinchenko

Abstract

Production of π^+, K^+ mesons in interactions of the argon beam with the kinetic energy 3.2 AGeV with the *C*, *Al*, *Cu*, *Sn*, *Pb* targets was studied with the BM@M detector at the Nuclotron. The analysis procedure is described in details. Results on π^+, K^+ meson yields have been obtained and compared with model predictions and data available.

BM@N configuration in the argon beam run

The technical run of the BM@N detector was performed with the argon beam in March 2018. The view of the BM@N setup used in the run is presented in Fig. 1. The configuration of the central tracker was based on three planes of forward silicon detectors and six stations consisted of GEM detectors with the size of 163x45 cm^2 [GEMTDR]. The GEM tracking stations were arranged to cover the upper part of the magnet acceptance. The beam passed the GEM detectors through the arc holes (Fig. 2). Each successive GEM station was rotated by 180^o around the vertical axis. It was done to have the opposite electron drift direction in the successive stations in order to avoid a systematic shift of reconstructed tracks due to the Lorentz angle in the magnetic field. The research program was devoted to measurements of inelastic reactions $Ar+A \rightarrow X$ with the beam kinetic energy of 3.2 AGeV and different targets: *C*, *Al*, *Cu*, *Sn*, *Pb*.

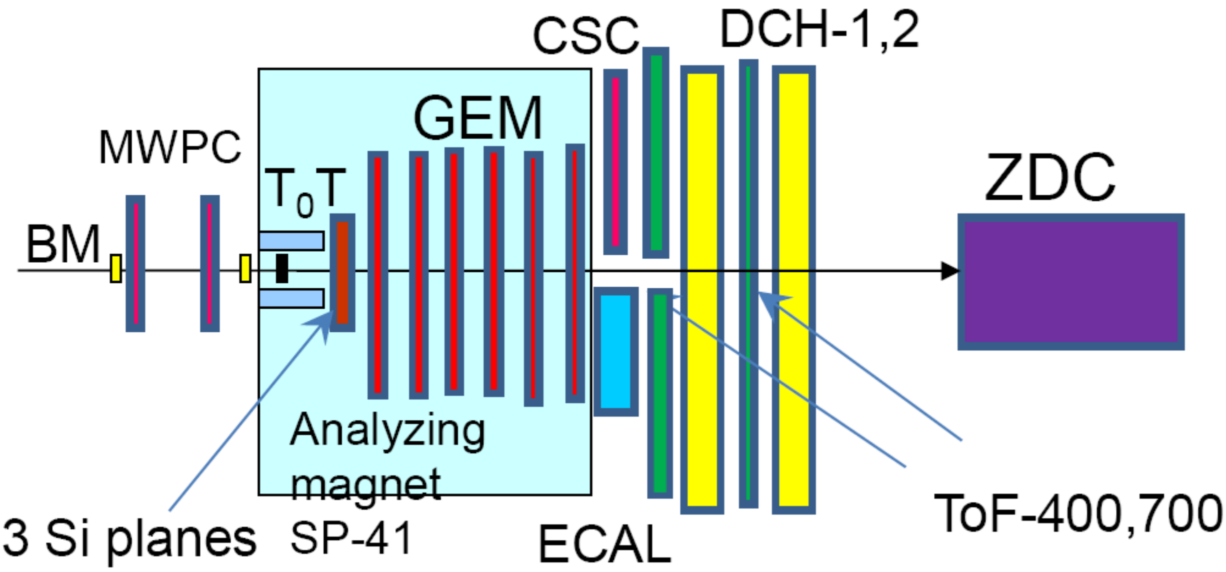

Fig. 1. BM@N set-up in the argon beam run.

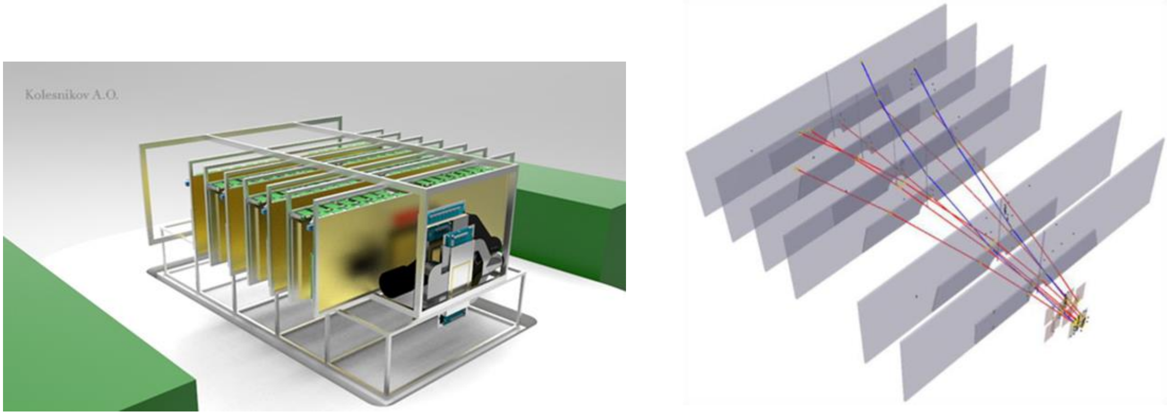

Fig.2. Left: Schematic view of the central tracking detectors (3 forward silicon and 6 GEM detectors). Right: Event of Ar+A→X interaction reconstructed in the central tracking detectors.

In the present analysis the experimental data from the forward silicon detectors, GEM detectors, trigger barrel BD and silicon multiplicity FD detectors around the target, beam and T0 counters and two sets of the time-of-flight detectors ToF-400 and ToF-700 were analyzed. To confirm matching of extrapolated tracks reconstructed in the central detectors to the ToF detectors, hits in the outer tracking detectors: cathode strip chamber CSC or drift chambers DCH were used. The argon beam intensity was few 10^5 per the spill, the spill duration was 2-2.5 sec. The magnetic field in the center of the analyzing magnet was 0.61 T. Number of triggered events, beam fluxes and integrated luminosities collected in interactions of the argon beam with different targets are given in Table 1a and 1b for the ToF-400 and ToF-700 data sample, respectively. The data samples included "good quality" runs where the CSC (DCH) and ToF-400 (ToF-700) detectors were fully operational.

Event reconstruction

The track reconstruction method was based on the so-called "cellular automaton" approach [CBM1]. The tracks found were used to reconstruct primary and secondary vertices using the "KF-particle" formalism [CBM2]. $\pi+$ and $K+$ were identified using the time of flight from the ToF detectors, the length of the trajectory and the momentum reconstructed in the central tracker. The $\pi+$ and $K+$ candidates should originate from the primary event vertex, correlate with hits in the CSC / DCH detectors and match hits in the ToF-400 / ToF-700 detectors. Herewith, the CSC (DCH) hits were used to confirm the quality of the tracks matched to ToF-400 (ToF-700) hits. Events were recorded with different conditions on the minimum number of fired channels in the barrel BD and multiplicity silicon FD trigger detectors, ranging from zero to 4.

Table 1a. Number of triggered events, beam fluxes and integrated luminosities collected in interactions of the argon beam of 3.2 AGeV with different targets (ToF-400 data sample).

Interactions, target thickness	Number of triggers / 10^6	Integrated beam flux / 10^7	Integrated luminosity / 10^{30} cm^{-2}
Ar+C (2 mm)	9.5	9.1	2.06
Ar+Al (3.33 mm)	24.1	11.5	2.30

Ar+Cu (1.67 mm)	24.5	12.7	1.79
Ar+Sn (2.57 mm)	23.8	11.6	1.11
Ar+Pb (2.5 mm)	11.7	6.1	0.50

Table 1b. Number of triggered events, beam fluxes and integrated luminosities collected in interactions of the argon beam of 3.2 AGeV with different targets (ToF-700 data sample).

Interactions, target thickness	Number of triggers / 10^6	Integrated beam flux / 10^7	Integrated luminosity / 10^{30} cm^{-2}
Ar+C (2 mm)	9.4	8.7	1.97
Ar+Al (3.33 mm)	21.6	10.2	2.05
Ar+Cu (1.67 mm)	21.0	11.3	1.60
Ar+Sn (2.57 mm)	19.0	9.5	0.91
Ar+Pb (2.5 mm)	9.7	4.9	0.40

π+ and *K*+ selection criteria:

- Each track has at least 4 hits in GEM detectors (6 detectors in total), where hit is a combination of two strip clusters on both readout sides (*X* and *X′* views) on each detector [GEMTDR]
- Tracks are originated from the primary event vertex, the deviation of the reconstructed vertex from the position of the target along the beam direction $-3.4<|Z_{vertex} – Z_0|<1.7$ cm. A harder upper limit is aimed to remove background due to interactions in a scintillator counter behind the target.
- Distance of the closest approach of tracks from the vertex in the direction perpendicular to the beam at Z_{vertex}: dca < 1 cm
- $\chi 2$ / ndf for tracks from the primary vertex < 3.5^2
- Momentum range of positive tracks: p_{pos}>0.5, 0.7 GeV/*c* for analysis of the ToF-400 and ToF-700 data, respectively
- Correlation of extrapolated tracks with the CSC / DCH hits as well as with the ToF-400 / ToF-700 hits should be within ±2.5σ of the residual distributions.

Event simulation:

The Monte Carlo event samples of *Ar+A* collisions were produced with the DCM-SMM event generator. The passage of particles through the setup volume was simulated with the GEANT program integrated into the BmnRoot software framework. To properly describe the GEM detector response in the magnetic field, the microsimulation package Garfield++ was used. The package gives very detailed description of the processes inside the GEM detector, including the drift and diffusion of released electrons in electric and magnetic fields and the electron multiplication in GEM foils, so that the output signal from the readout plane can be reproduced. To speed up the simulation, dependencies of the Lorentz shifts and the charge distributions on the readout planes on the drift distance were parameterized and used in the GEM digitization part of the BmnRoot package. The details of the detector alignment, Lorenz shift corrections are described in the paper [DeuteronPaper]. Examples of experimental and Monte Carlo distributions of the distance of the closest approach of tracks to the vertex, χ^2 of reconstructed tracks, number of tracks reconstructed in the primary vertex, number of hits per track are presented in Fig.3a. Distributions of the total momentum p and transverse momentum p_T of π+ and K+ for ToF-400 and ToF-700 data and simulation are presented in Fig.3b and 3c, respectively.

The detector effects in simulation were controlled by reproducing the track reconstruction efficiency evaluated from data. Efficiency distributions in 3 Si and 6 GEM stations measured with reconstructed experimental tracks are shown in Fig.4. For each station they were estimated using the following approach:

1. Select good quality tracks with the number of hits per track (excluding the station under study) not less than N;
2. Check that track crosses the detector area, if yes, add one track to the denominator;
3. If there is a hit in the detector, which belongs to the track, add one track to the numerator;
4. Detector efficiency is equal to the ratio of number of tracks in numerator to number of tracks in denominator.

These efficiencies were applied to reduce the number of hits of tracks reconstructed in simulation. The experimental and simulated distributions of Si and GEM hit residuals to tracks in X and Y projections are presented in Fig.5a and Fig.5b, respectively. The RMS of distributions are in a reasonable agreement between data and simulation. The mean values and sigma of the residuals of CSC hits in the X and Y projections with respect to reconstructed positive tracks identified in ToF-400 are given in Fig.6a - Fig.6d in dependence on the particle momentum. The mean values and sigma of the residuals of ToF-400 hits in the X and Y projections with respect to reconstructed positive tracks are given in Fig.7a - Fig.7d in dependence on the particle momentum. The mean values and sigma of the residuals of DCH hits in the X and Y projections with respect to reconstructed positive tracks identified in ToF-700 are given in Fig.8a - Fig.8b in dependence on the particle momentum. The mean values and sigma of the residuals of ToF-700 hits in the X and Y projections with respect to reconstructed positive tracks are given in Fig.9a - Fig.9b in dependence on the particle momentum.

Signals of π+ and K+ in experimental data:

The mass squared spectrum of positive particles identified in ToF-400 and ToF-700 in experimental and simulated events of $Ar+A$ interactions are illustrated in Fig.10a and 10b, respectively. Signals of π+ and K+ were extracted in windows of the mass squared from -0.09 to 0.13 $(GeV/c^2)^2$ and from 0.18 to 0.32 $(GeV/c^2)^2$, respectively. Numbers of π+ and K+ were taken from the content of the histogram bins within the corresponding mass windows. To estimate the background in the π+ and K+ mass windows, the "mixed event" method was used, i.e. the shape of the mass squared background distribution was evaluated by matching tracks to hits in the ToF-400 and ToF-700 detectors originated from independent events. Signals of π+ and K+ in the intervals of the transverse momentum p_T and rapidity y_{lab} were reconstructed using the same procedure. The errors of the π+ and K+ signals include the uncertainty of the background subtraction. The statistical and systematic errors were calculated according to the formula: $sig=hist-bg$, $err(stat)=\sqrt{hist+bg}$, assuming the background uncertainty of $\sqrt{bg}$. Here *hist* and *bg* denote the histogram integral and the background integral within the π+ and *K*+ mass squared windows. To estimate the π+ and *K*+ signal systematic errors due to the background subtraction method, the distributions were fitted to the 1st degree polynomial (background) in the mass squared range -0.14-0.4 (GeV/c^2)^2. The variation of the background integral in the π+ *(K+)* mass squared window taken from mixed events relative to the *bg* integral taken from the fit of the mass squared spectra was treated as a systematic error.

The π+ and *K*+ mass squared windows were excluded from the fit. Spectra of mass squared shown in Fig.10c and 10d in bins of y of π+ and K+ identified in ToF-400 in Ar+Cu interactions illustrate the background subtraction method using a linear fit. The mixed event method is illustrated in Fig.10e and 10f. Spectra of mass squared in bins of rapidity y of π+ and K+ identified in ToF-400 in Ar+Sn interactions: left) experimental events, right) simulated events. Background (blue histogram) is taken from mixed events and normalized to the red signal histogram in the mass squared range between the π+ and K+ peaks and above the K+ peak.

The statistics of π+ and *K*+ reconstructed in ToF-400 (ToF-700) in *Ar+C, Ar+Al, Ar+Cu, Ar+Sn, Ar+Pb* interactions are summarized in Table 2. Number of reconstructed π^+ *(K+)* in interactions of 3.2 AGeV argon beam with *C, Al, Cu, Sn, Pb* targets in bins of y_{lab} and p_T are shown in Fig. 11a (11b) for ToF-400 data. The corresponding 2-dimentional (y_{lab}, p_T) distributions are given in Fig.11c and 11d.

Table 2. Signals of π+ and K+ mesons reconstructed in ToF-400 and ToF-700 in argon-nucleus interactions. The error presents the statistical uncertainty.

Target	***ToF-400***				
	C	***Al***	***Cu***	***Sn***	***Pb***
π+	4020±66	21130±152	28010±175	32060±186	22420±156
K+	45±10	278±25	538±31	729±36	570±32
Target	***ToF-700***				
	C	***Al***	***Cu***	***Sn***	***Pb***
π+	1070±34	5640±80	8090±95	9450±104	6830±86
K+	31±6	117±16	193±21	346±23	221±20

π+/ *K*+ reconstruction efficiency from simulation:

The π+ / *K*+ reconstruction efficiency is the ratio of the number of reconstructed π+ / *K*+ to the number of generated ones in the intervals of (p_T,*y*), where *y* is measured in the laboratory frame (y_{lab}). The reconstruction efficiency can be decomposed into the following components: $\varepsilon_{rec} = \varepsilon_{acc} \cdot \varepsilon_{cuts}$. The definition of every term is given in Table 4 and their determination procedure is as follows.

After the event simulation and reconstruction the successfully reconstructed $\pi+$ / $K+$ were counted in the numerator N_{acc}. The detector acceptance was taken as N_{acc} / N_{gen}, where N_{gen} is the total number of generated MC events. The number of $\pi+$/ $K+$ after applying kinematic and spatial cuts (N_{cuts}) gave the "selection cuts" efficiency with respect to the number of accepted ones from above.

Table 4. Decomposition of the $\pi+$ / $K+$ reconstruction efficiency.

Reconstruction efficiency	$\varepsilon_{rec} = \varepsilon_{acc} \cdot \varepsilon_{cuts}$
$\pi+$/ $K+$ geometrical acceptance in detectors	$\varepsilon_{acc} = N_{acc}\,(y,p_T) / N_{gen}\,(y,p_T)$
Efficiency of reconstruction of $\pi+$/ $K+$ within the detector geometrical acceptance after applying kinematic and spatial cuts	$\varepsilon_{cuts} = N_{cuts}(y,p_T) / N_{acc}(y,p_T)$

The actual values of the efficiencies (ε_{acc}, ε_{cuts}) and combined reconstruction efficiencies ε_{rec} calculated in the y, p_T and 2-dinetional (y, p_T) bins are shown in Figs. 12a – 12b for π^+, K^+ mesons reconstructed in ToF-400 in *Ar+A* interactions.

Trigger efficiency:

Different conditions on the minimum number of fired channels in the barrel BD and multiplicity silicon FD trigger detectors, ranging from zero to 4 were applied to record experimental data. The mean efficiency ε_{trig} of the BD and FD trigger detectors for events with reconstructed π^+ / K^+ produced in interactions of the argon beam with the whole set of *C, Al, Cu, Sn, Pb* targets is given in Table 5a and 5b, respectively. The dependence of the BD and FD trigger efficiency on the number of tracks from the primary vertex for events with reconstructed π^+ / K^+ is presented in Fig.13a and 13b, respectively. The systematic errors used in the analysis cover the differences in the π+, K+ signals obtained by using the mean values of the trigger efficiency values instead of the efficiency dependences on the number of the vertex tracks and the Y position of the primary vertex. The trigger efficiency of BD (FD) detectors was evaluated using experimental event samples recorded with an independent trigger based on FD (BD): ε(BD>=m) = [N(BD>=m & FD>=n]/ N(FD>=n) for every target. The efficiency for the combined BD and FD triggers was calculated as a product of the BD and FD trigger efficiencies.

Table 5a. Mean BD trigger efficiency evaluated for events with reconstructed π^+ / K^+ in interactions of the argon beam with the whole set of *C, Al, Cu, Sn, Pb* targets.

Trigger / Target 3.2 AGeV π^+ mesons	***C***	***Al***	***Cu***	***Sn***	***Pb***
ε_{trig} (BD>=2)	0.80±0.03	0.96±0.01	0.98±0.01	0.99±0.01	0.99±0.01
ε_{trig} (BD>=3)	0.66±0.02	0.92±0.01	0.97±0.01	0.98±0.01	0.99±0.01
ε_{trig} (BD>=4)	0.48±0.02	0.88±0.01	0.95±0.01	0.97±0.01	0.98±0.01

Trigger / Target 3.2 AGeV, K^+ mesons	***C***	***Al***	***Cu***	***Sn***	***Pb***

ε_{trig} (BD>=2)	0.67±0.15	0.97±0.02	0.99±0.01	0.99±0.01	0.99±0.01
ε_{trig} (BD>=3)	0.67±0.15	0.96±0.02	0.98±0.01	0.99±0.01	0.99±0.01
ε_{trig} (BD>=4)	0.67±0.15	0.94±0.02	0.95±0.02	0.99±0.01	0.98±0.01

Table 5b. Mean FD trigger efficiency evaluated for events with reconstructed π^+ / K^+ in interactions of the argon beam with the whole set of *C, Al, Cu, Sn, Pb* targets.

Trigger / Target 3.2 AGeV π^+ mesons	***C***	***Al***	***Cu***	***Sn***	***Pb***
ε_{trig} (FD>=2)	0.28±0.01	0.40±0.01	0.56±0.01	0.65±0.01	0.73±0.01
ε_{trig} (FD>=3)	0.14±0.01	0.22±0.01	0.37±0.01	0.49±0.01	0.58±0.01
ε_{trig} (FD>=4)	0.08±0.01	0.11±0.01	0.23±0.01	0.34±0.01	0.46±0.01

Trigger / Target 3.2 AGeV, K^+ mesons	***C***	***Al***	***Cu***	***Sn***	***Pb***
ε_{trig} (FD>=2)	0.30±0.06	0.40±0.03	0.64±0.03	0.74±0.03	0.82±0.03
ε_{trig} (FD>=3)	0.17±0.04	0.23±0.02	0.45±0.03	0.61±0.03	0.73±0.03
ε_{trig} (FD>=4)	0.08±0.03	0.12±0.02	0.35±0.03	0.44±0.03	0.58±0.03

Luminosity uncertainty (see separate document Lumi.pdf)

Impact parameter distribution:

Distributions of the impact parameters of minimum bias interactions generated with the DCM-SMM model all generated events with *π+ (K+)* are shown in Fig.14a and 14b. The impact parameter distributions for events with *π+ (K+)* in the measured kinematical range as well as the impact parameters of simulated events with reconstructed *π+* (K+) are presented for comparison. The measured kinematical ranges in the rapidity spectra of π^+ and *K+* generated with the DCM-SMM model in minimum bias interactions of the 3.2 AGeV argon beam with the Cu target, are given in Fig.14c.

Evaluation of *π+* / *K+* cross sections and spectra:

The inclusive cross section $\sigma_{\pi+}$ and yield $Y_{\pi+}$ of π+ production in *Ar+C, Ar+Al, Ar+Cu, Ar+Sn,Ar+Pb* interactions are calculated in bins of *y* (p_T) according to the formulae:

$$\sigma_{\pi+}(y, p_T)= N_{rec}(y,p_T) / (\varepsilon_{rec} (y,p_T)\cdot\varepsilon_{trig}\cdot L) \qquad Y_{\pi+} (y,p_T) = \sigma_{\pi+} (y,p_T) / \sigma_{inel}$$

where *L* is the luminosity (Table 1), N_{rec} – the number of reconstructed *π+* (Table 2), ε_{rec} – the combined efficiency of the *π+* reconstruction, ε_{trig} – the trigger efficiency (Table 5), σ_{inel} – the cross section for minimum bias inelastic *Ar+A* interactions (Table 7). The same formulas are used to calculate the *K+* inclusive production cross section and yield in bins of *y* (p_T). The cross sections in (y, p_T) bins are calculated as weighted averaged of the results obtained with ToF-400 and ToF-700 data taking into account the statistical errors (w ~ $1/\sigma^2$). The cross sections for inelastic *Ar+Al, Ar+Cu, Ar+Sn, Ar+Pb* interactions are taken from the predictions of the DCM-SMM model which are consistent with the results calculated by the formula: $\sigma_{inel} = \pi R_0^2 (A_P^{1/3} + A_T^{1/3})^2$, where R_0 = 1.2 fm is an effective nucleon radius, A_P and A_T are atomic numbers of the beam and target nucleus [HadesL0]. The uncertainties for *Ar+Al, Ar+Cu, Ar+Sn, Ar+Pb* inelastic cross sections are estimated by using the alternative formula: $\sigma_{inel} = \pi R_0^2 (A_P^{1/3} + A_T^{1/3} - b)^2$ with R_0 = 1.46 fm and b = 1.21 [AngelovCC].

Table 7. Inelastic cross sections for argon-nucleus interactions.

Interaction	***Ar+C***	***Ar+Al***	***Ar+Cu***	***Ar+Sn***	***Ar+Pb***
Inelastic cross section, mb	1470±50	1860±50	2480±50	3140±50	3970±50

The yields of $\pi+$ / $K+$ in minimum bias *Ar+C, Ar+Al, Ar+Cu, Ar+Sn, Ar+Pb* interactions are measured in the kinematic range on the transverse momentum of $0.1<p_T<0.6$ GeV/c for $\pi+$ ($0.1<p_T<0.5$ GeV/c for $K+$) and the rapidity in the laboratory frame of $1.5<y_{lab}<3.2$ for $\pi+$ ($1.0 <y_{lab}<2.0$ for $K+$). The rapidity of the beam-target nucleon-nucleon CM system calculated for an interaction of the argon beam with the kinetic energy of 3.2 GeV/nucleon with a fixed target is y_{CM}=1.08. The transformation of the y distribution to c.m.s. gives $y^*=y_{lab}-y_{CM}$. The differential spectra of the $\pi+$ ($K+$) yields in y_{lab} are measured in the $\pi+(K+)$ transverse momentum range of $0.1<p_T<0.6$ GeV/c ($0.1<p_T<0.5$ GeV/c). The corrected differential y_{lab} spectra of $\pi+$ / $K+$ yields are presented in Figs. 15a and 15b, respectively. Due to low statistics of the $K+$ meson signal in Ar+C interactions, the results are given only for the whole measured range in y_{lab} and p_T. Predictions of the DCM-SMM, URQMD and PHSD models are shown for comparison. The corrected invariant differential p_T spectra of π^+, K^+ yields are presented in Fig. 16a, 16b-c, respectively. The measured spectra of the $\pi+$ / $K+$ yields in p_T are parameterized by the form: $1/p_T \cdot d^2N/dp_T dy = N \cdot exp(-(m_T - m_{\pi+})/T)$, where $m_T = \sqrt{(m_{\pi+}^2 + p_T^2)}$ is the transverse mass, the normalization N and the inverse slope parameter T are free parameters of the fit, dy corresponds to the measured y_{lab} range. In Fig.17a and 17b the inverse slopes T of the experimental invariant p_T spectra of $\pi+$ / $K+$ mesons are compared with t predictions of the DCM-SMM, URQMD and PHSD models. In Table 12b the inverse slopes T of the invariant p_T spectra of $K+$ mesons are given for the whole measured range in y_{lab} and p_T.

Systematic uncertainties:

The systematic error of the $\pi+$ / $K+$ yields in every p_T and y bin is calculated as a quadratic sum of uncertainties coming from the following sources:

- Sys1: Systematic error of the trigger efficiency evaluated as a function of the number of tracks from the primary vertex and the primary vertex position.
- Sys2: Systematic errors of the reconstruction efficiency due to the remaining difference in the X/Y primary vertex distribution in the simulation relative to the experimental data.
- Sys3: Systematic errors of the background subtraction under the $\pi+$ and $K+$ signals in the mass squared spectra of identified particles as described in section on **Signals of π+ and K+ in experimental data.**

The *π*+ / *K*+ yield normalization uncertainty calculated as a quadratic sum of uncertainties of the trigger efficiency, tracking efficiency, luminosity and inelastic nucleus-nucleus cross section. The normalization error is valid for the whole measured kinematical range. The luminosity uncertainty is estimated to be within 2%. The normalization uncertainty of the trigger efficiency is 28% for *K*+ detection in Ar+C interactions and between 7.5% (Ar+Al) and 4% (Ar+Pb) for *K*+ detection in interactions of argon with more heavy targets. The trigger efficiency uncertainty for *π*+ detection ranges between 4.5% (Ar+C) and 0.9% (Ar+Pb). The uncertainty of the central tracking detector efficiency is estimated to be within 3%. The uncertainty of matching of extrapolated tracks with the CSC (DCH) hits as well as with the ToF-400 (ToF-700) hits is within 5%. The tracking and outer detector uncertainties are estimated from the remaining differences between the efficiencies obtained in experimental and Monte-Carlo events.

Relative difference of *π*+ *(K+)* yields measured in (y,p_T) bins using combined ToF-400 and ToF-700 data are given in Fig.14d and 14e, respectively. Relative difference of *π*+ *(K+)* yields measured in (y,p_T) bins originated from different sources of systematic uncertainties are given in Fig.14f and 14i, respectively. The average values of systematic uncertainties *π*+ *(K+)* yields in Ar+C, Al, Cu, Sn, Pb interactions are summarized in Table 10.

Table 10. Total systematic uncertainty of the *π*+ and K+ yields measured argon-nucleus interactions.

Target / Systematics		*π*+				Target		***K+***			
	C sys%	***Al*** sys%	***Cu*** sys %	***Sn*** sys%	*Pb* sys%		***C*** sys%	***Al*** sys%	***Cu*** sys%	***Sn*** sys%	***Pb*** sys%
Sys1-Sys3	14	11	12	9	9		28	26	14	12	16
Norm (trigger + tracking + luminosity)	7.8	6.3	6.2	6.2	6.2		29	10	8.4	7.6	7.4

Integrated yields and cross sections:

The integrated yields of *π*+ / *K*+ produced in the kinematic range of $0.1<p_T<0.6$ GeV/*c* for *π*+ ($0.1<p_T<0.5$ GeV/*c* for *K*+) and $1.5 <y_{lab}<3.2$ for *π*+ ($1.0 <y_{lab}<2.0$ for *K*+) in minimum bias *Ar+C, Al, Cu, Sn, Pb* interactions are summarized in Tables 12a and 12b. To extrapolate the measured yields to the full kinematic range the predictions of the DCM-SMM model are used. The rapidity spectra of *π*+ and *K*+ generated in the DCM-SMM model are shown in Fig.14c. The model extrapolation factors, the full yields of the *π*+ and K+ production in *Ar+C, Ar+Al, Ar+Cu, Ar+Sn, Ar+Pb* minimum bias interactions with beam energy of 3.2 AGeV are also given in Tables 12a and 12b. The ratios of *K*+ to *π*+ yields are given in Table 12b.

Table 12a. Extrapolation factors to the full kinematic range and *π*+ yields for 3.2 AGeV argon-nucleus data in the measured and full kinematical ranges. The first errors given are statistical, the second errors are systematic.

3.2 AGeV, *π*+	***C***	***Al***	***Cu***	***Sn***	***Pb***
DCM-SMM extrap. factor				4.98	5.64

	3.43	3.86	4.51		
Yield in 0.1<p_T<0.6 GeV/c, 1.5<y_{lab}<3.2	0.275±0.006±0.027	1.00±0.01±0.07	1.14±0.01±0.08	1.28±0.01±0.09	1.25±0.01±0.085
Yield in the full kin. range	0.943±0.019±0.092	3.86±0.04±0.27	5.15±0.05±0.35	6.35±0.05±0.44	7.03±0.07±0.48

Table 12b. Extrapolation factors to the full kinematic range , *K*+ yields and K+ to *π*+ yield ratios for 3.2 AGeV data in the measured and full kinematical ranges. The first errors given are statistical, the second errors are systematic. Also the inverse slope parameters *T* of the invariant p_T spectra are given.

3.2 AGeV *K*+	***C***	***Al***	***Cu***	***Sn***	***Pb***
DCM-SMM extrap. factor	2.33	2.51	2.84	3.21	3.67
Yield in 0.1<p_T<0.5 GeV/c, 1.0<y_{lab}<2.0	0.0094±0.0018±0.0035	0.0390±0.0028±0.0061	0.0417±0.0021±0.0066	0.056±0.0022±0.0075	0.051±0.0022±0.0092
Yield in the full kin. range	0.0219±0.0042±0.0081	0.098±0.007±0.015	0.119±0.006±0.019	0.180±0.007±0.024	0.188±0.008±0.034
K+/ *π*+ ratio, measured range	0.0343±0.0066±0.0125	0.0390±0.0028±0.0055	0.0366±0.0019±0.0053	0.0439±0.0018±0.0051	0.0411±0.0018±0.0068
K+/ *π*+ ratio, full kin. range	0.0233±0.0045±0.0085	0.0253±0.0018±0.0035	0.0230±0.0012±0.0033	0.0283±0.0012±0.033	0.0268±0.0012±0.0044
K+ inverse slope T, MeV measured range	73±14±13	80±7±5	81±5±5	81±5±4	78±5±4

In general, the transport models describe the shape of the differential spectra on *y* and p_T, but predict more abundant yields of *π*+ and *K*+ in Ar+C interactions than measured in the experiment. The BM@N results could be compared with the results of other experiments studied argon-nucleus interactions at lower energies, shown in Table 13.

Table 13. Yields of K+ , π+ production and effective inverse slopes of invariant m_T spectra measured in in interactions of light and medium nucleus.

Interacting nucleus / Beam kinetic energy / Experiment	*π*+ , K+ yields	*K*+ / *π*+ yield ratio, $\cdot 10^{-2}$	T_{eff} at $y^* = 0$, MeV, *K*+ / *π*+
Ar+KCl, 1.76 AGeV, [HADES1]	3.9±0.1±0.1 (π-) (2.8 ± 0.2) $\cdot 10^{-2}$ (K+)		82.4 +9.1−4.6 (π-) 89 ± 1 ± 2 (K+)
Ar+KCl, 1.93 AGeV	3.9±0.14±0.08 (π+)		
Ni+Ni, 1.93 AGeV [FOPI1,FOPI3]	$3.6 \cdot 10^{-2}$ (K+, Apart= 46.5) $8.25 \cdot 10^{-2}$ (K+, Apart = 75)	7.59 ± 0.49 $\cdot 10^{-3}$ (Apart = 46.5)	101.9 ± 1.0
Ni+Ni, , 1.93 AGeV	87±10 mb, $3 \cdot 10^{-2}$ (K+)		97±7 (non-central)

[KaoS1, KaoS2]			107±10 (central)

Summary

Production of $\pi+$ and $K+$ in interactions of the argon beam with *C*, *Al*, *Cu*, *Pb* targets was studied with the BM@N detector. The analysis procedure is described including details of the $\pi+$ reconstruction, efficiency and systematic uncertainty evaluation. First physics results are presented on $\pi+$ / $K+$ yields in minimum bias argon-nucleus interactions at the beam kinetic energies of 3.2 AGeV. The results are compared with models of nucleus-nucleus interactions.

Bibliography

[DeuteronPaper] D.Baranov et al., First Results from BM@N Technical Run with Deuteron Beam, Phys. Part. Nucl. Lett. 15, no. 2, 148 (2018)
[GEMconf] https://bmn-wiki.jinr.ru/bin/view/Run/2.%20Run%20Control/2.1%20Run%207/BM%40N%20Session%20%28GEM%29/
[GEMTDR] https://bmn-wiki.jinr.ru/bin/view/Doc/4.%20Documents/4.4%20BM%40N%20TDR/GEM%20tracker/
[CBM1] V. Akishina and I. Kisel. Time-based cellular automaton track finder for the CBM experiment - 2015. J. Phys.: Conf. Ser. 599, 012024
[CBM2] S. Gorbunov and I. Kisel. Reconstruction of decayed particles based on the Kalman filter - 2007. CBM-SOFTnote--003
[GenisPart] Result of Genis Musulmanbekov, private communication
[AnikinaCC] N.Anikina et al., Z.Phys.C, 25,(1984),1
[ArmutCC] D.Armutlijsky et al., P1-85-220, JINR, Dubna
[ArakelianCC] S.Arakelian et al., P1-83-354, JINR, Dubna
[AngelovCC] H.Angelov et al., P1-80-473, JINR, Dubna
[HadesL0] Kalliopi Kanaki, PhD "Study of Λ *hyperon* production in *C+C* collisions at 2A GeV beam energy with the HADES spectrometer", 2007
[HADES1] G.Agakishiev et al., HADES Collaboration, Eur.Phys.J.A 47 (2011) 21.
[HADES2] G.Agakishiev et al., HADES Collaboration, Phys.Rev.C 80 (2009) 025209.
[HADES3] G.Agakishiev et al., HADES Collaboration, Phys.Rev.C 82 (2010) 044907
[FOPI1] D.Best et al., FOPI Collaboration, Nucl.Phys.A 625 (1997) 307-324
[FOPI2] N.Bastid et al., FOPI Collaboration, Phys.Rev.C 76 (2007) 024906
[FOPI3] K.Piasecki et al., FOPI Collaboration, Phys.Rev.C 99 (2019) 1, 014904.
[KaoS1] M.Menzel et al., KaoS Collaboration, Phys.Lett.B 495 (2000) 26-32.
[KaoS2] A.Forster et al., KaoS Collaboration, Phys.Rev.C 75 (2007) 024906.

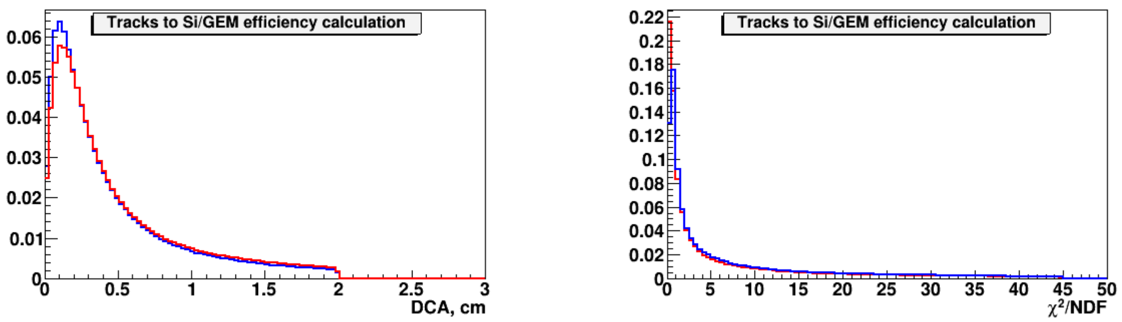

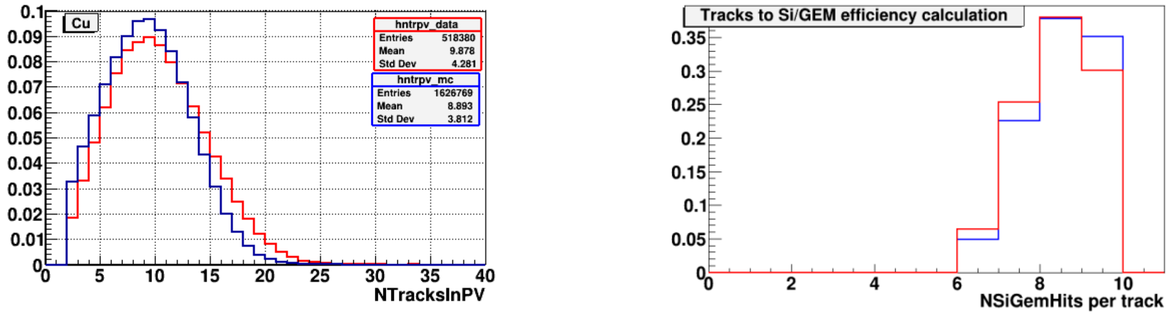

Fig.3a. *Ar+A* interactions at 3.2 AGeV argon beam energy: comparison of experimental distributions (red lines) and Monte Carlo GEANT distributions of events generated with the DCM-SMM model (blue lines): Distribution of the distance of the closest approach DCA between tracks and the vertex in the plane perpendicular to the beam direction; χ^2 of reconstructed tracks; number of tracks reconstructed in the primary vertex; number of hits per track reconstructed in 3 Si + 6 GEM detectors.

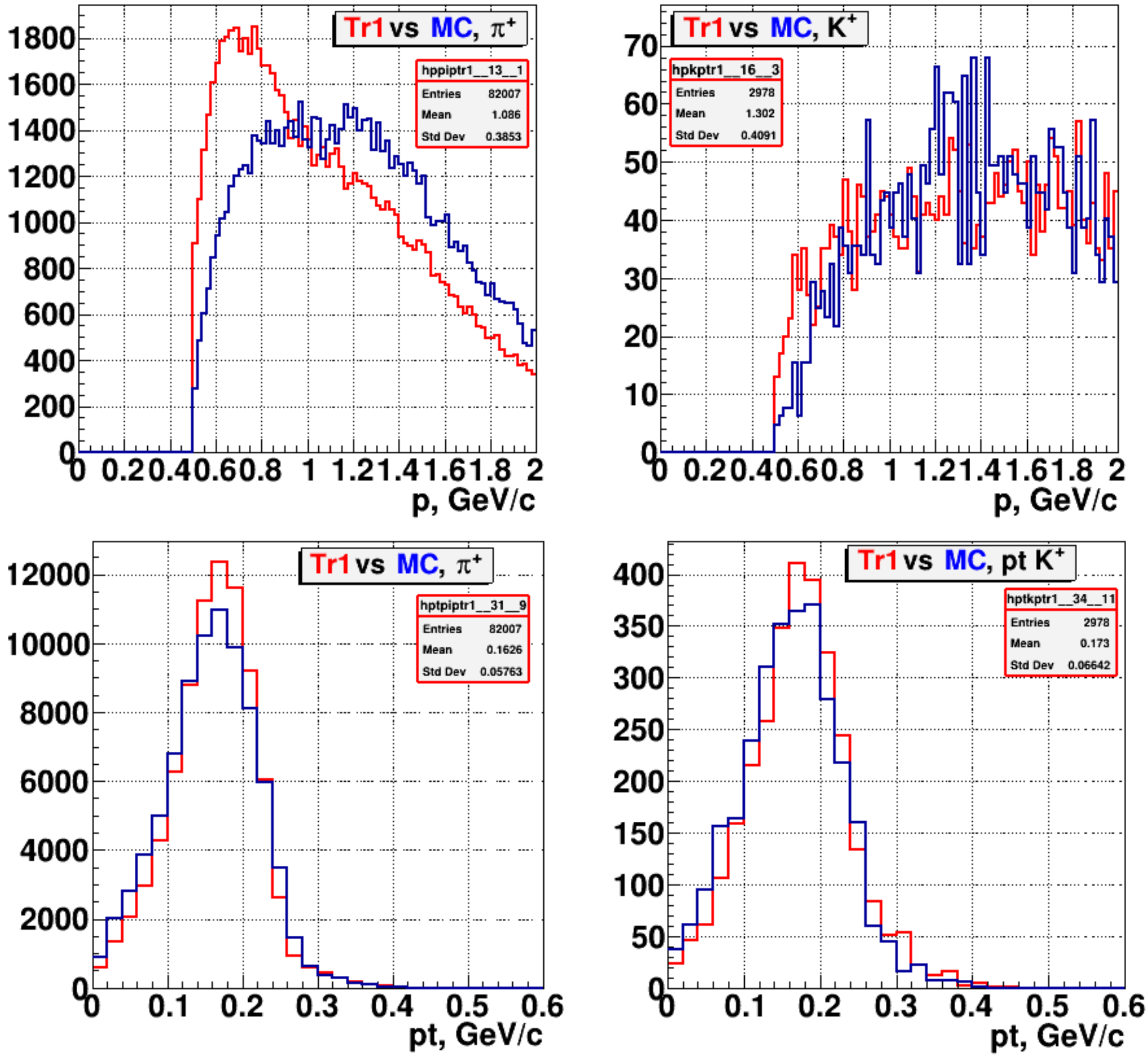

Fig. 3b. *Ar+A* interactions at 3.2 AGeV argon beam energy: comparison of ToF-400 experimental data (red curves) and DCM-SMM + GEANT Monte Carlo simulation (blue curves): total momentum of identified π^+ and K^+ (upper plots); transverse momentum of π^+ and K^+ (lower plots).

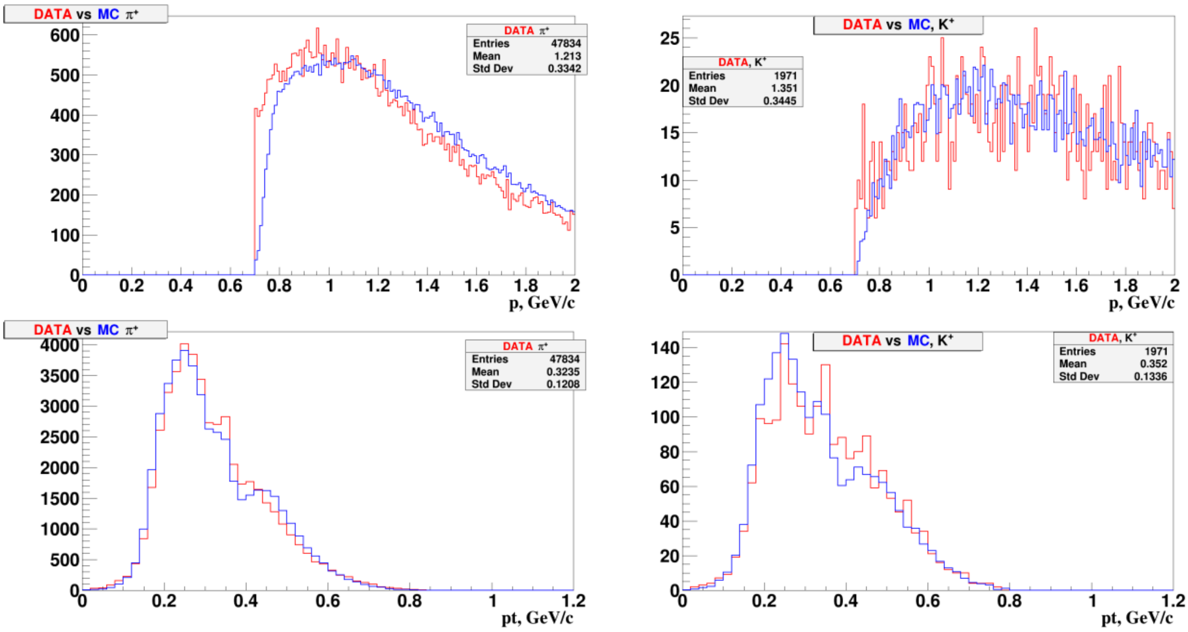

Fig. 3c. Ar+A interactions at 3.2 AGeV argon beam energy: comparison of ToF-700 experimental data (red curves) and DCM-SMM + GEANT Monte Carlo simulation (blue curves): total momentum of identified π+ and K+ (upper plots); transverse momentum of π+ and K+ (lower plots).

Si-1

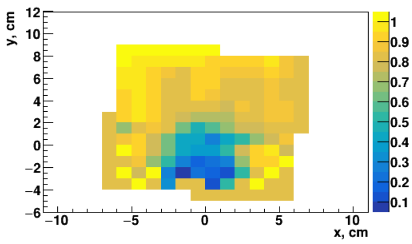

Si-2

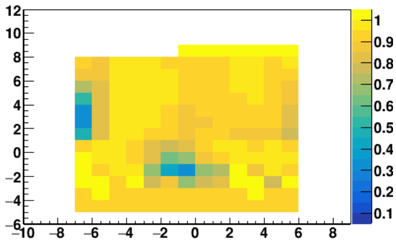

Si-3

GEM-1

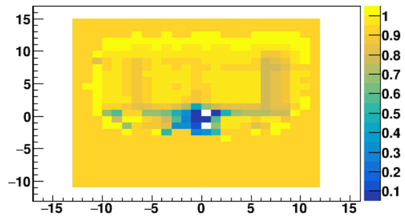

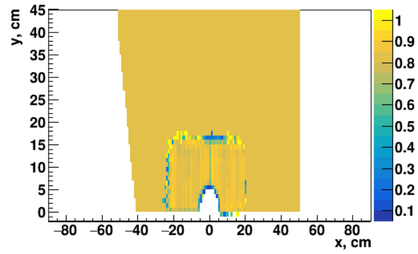

GEM-2

GEM-3

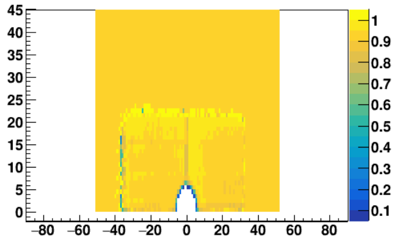

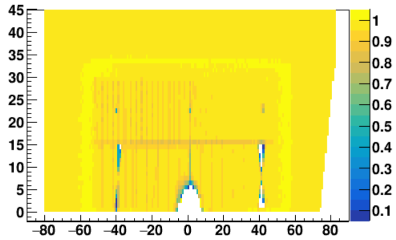

GEM-4

GEM-5

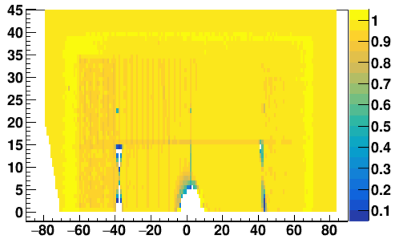

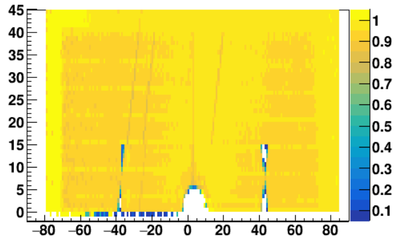

GEM-6

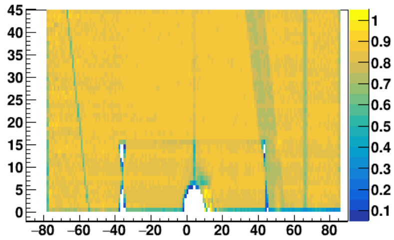

Fig. 4. 2-dimentional efficiency distributions in 3 Si and 6 GEM stations measured with experimental tracks and implemented into Monte Carlo simulation.

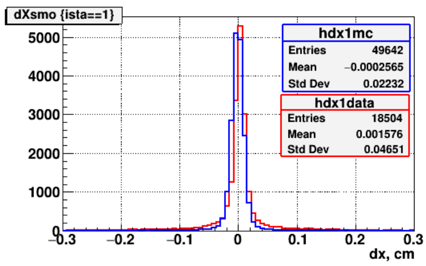

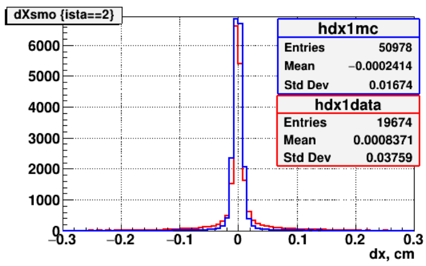

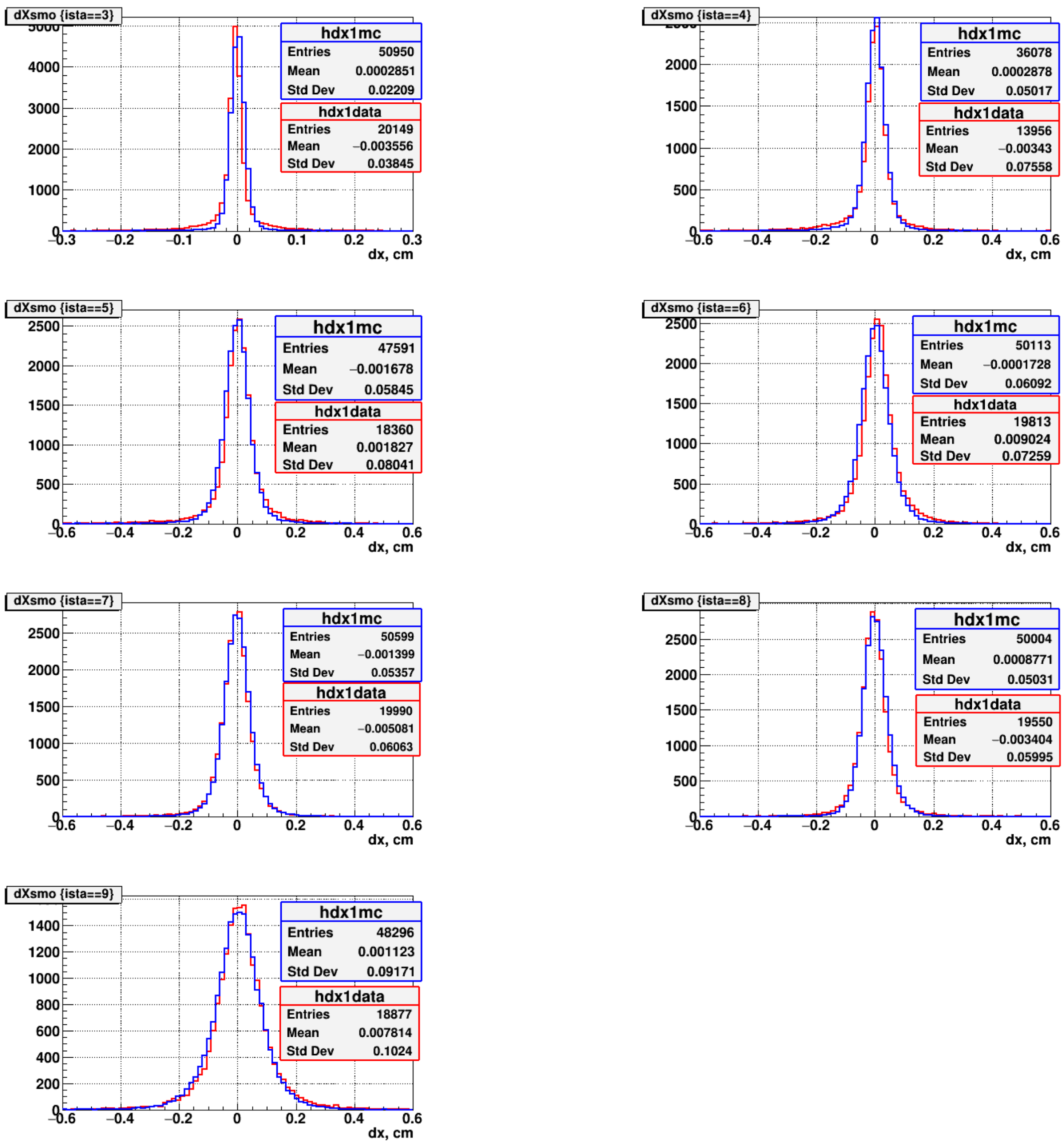

Fig. 5a. Residual distributions of hits in X projection with respect to reconstructed tracks in 3 Si (ista=1-3) and 6 GEM detectors (ista=4-9): experimental data (red histograms), simulated tracks (blue histograms).

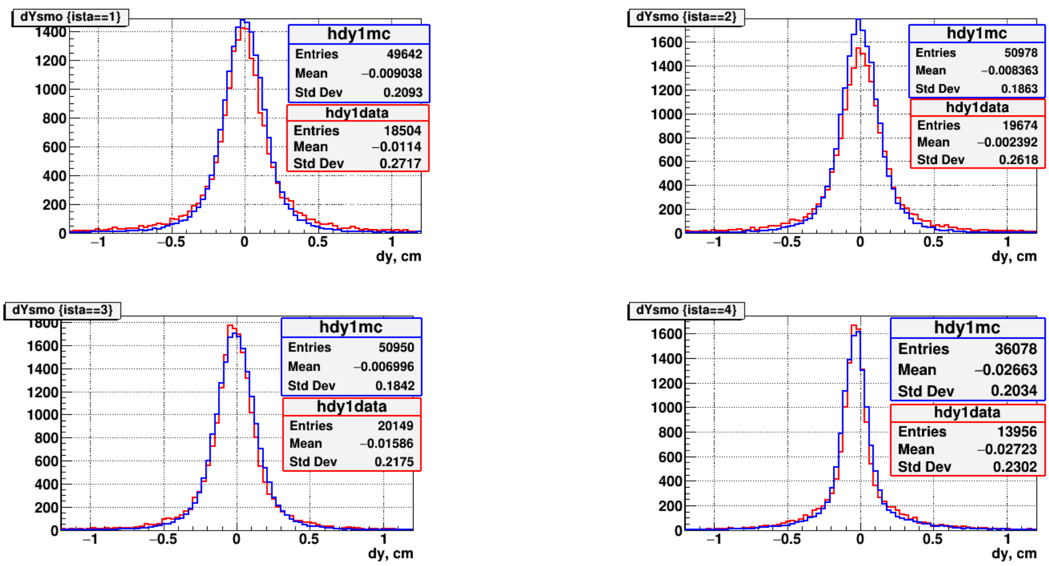

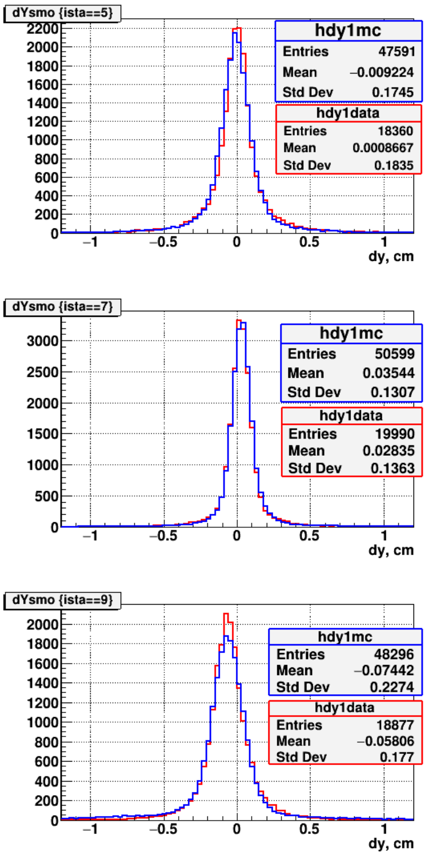

Fig. 5b. Residual distributions of hits in Y projection with respect to reconstructed tracks in 3 Si (ista=1-3) and 6 GEM detectors (ista=4-9): experimental data (red histograms), simulated tracks (blue histograms).

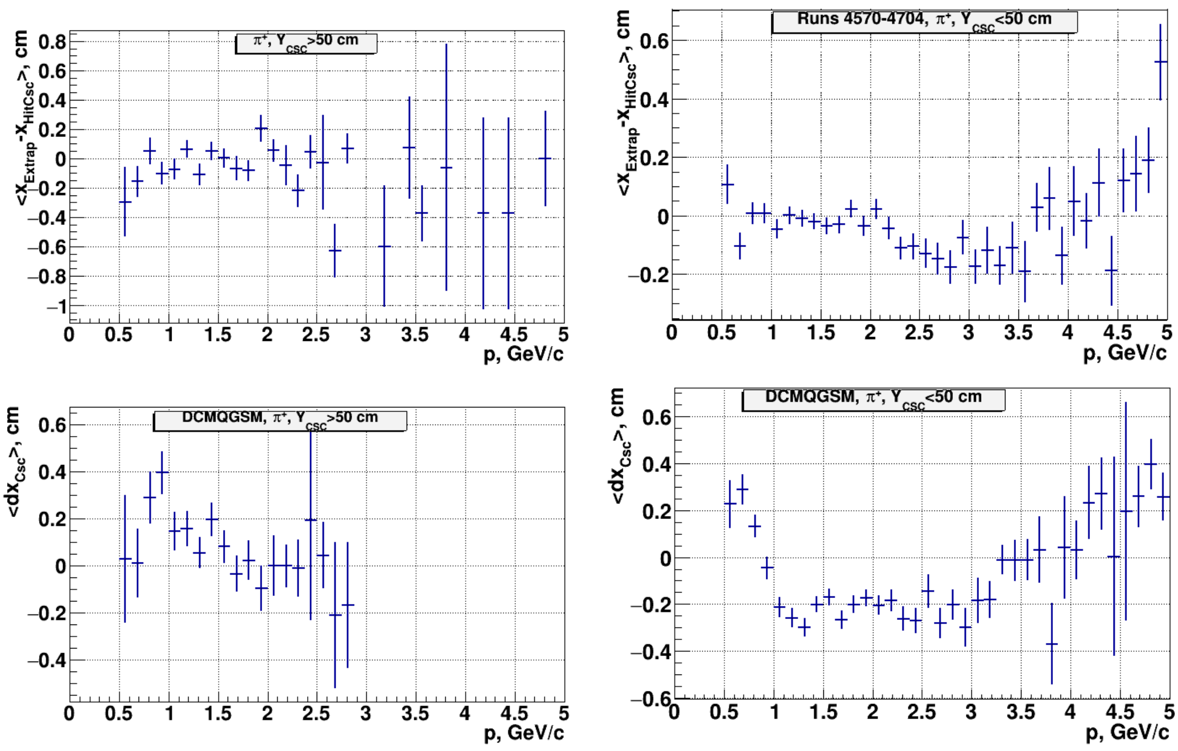

Fig. 6a. ToF-400 data and simulation: Mean values of residuals of CSC hits in X projection with respect to reconstructed positive tracks in dependence on the particle momentum for two ranges in Y: upper plots experimental data, lower plots – simulated tracks.

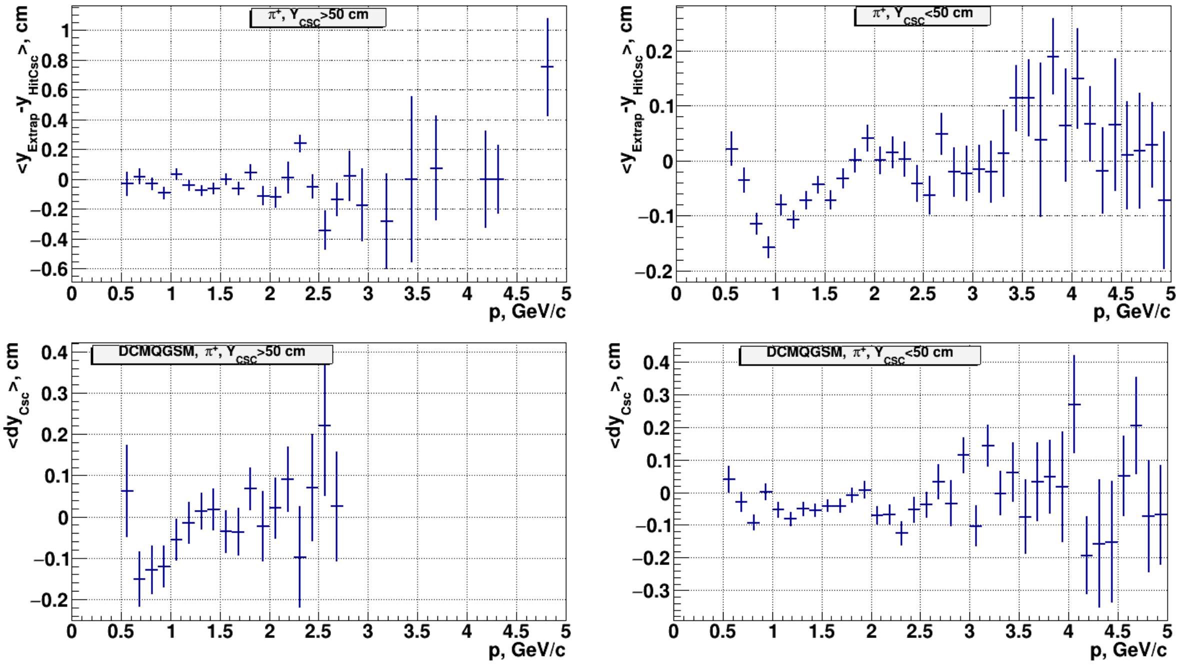

Fig. 6b. ToF-400 data and simulation: Mean values of residuals of CSC hits in the Y projection with respect to reconstructed positive tracks in dependence on the particle momentum for two ranges in Y: upper plots - experimental data, lower plots – simulated tracks.

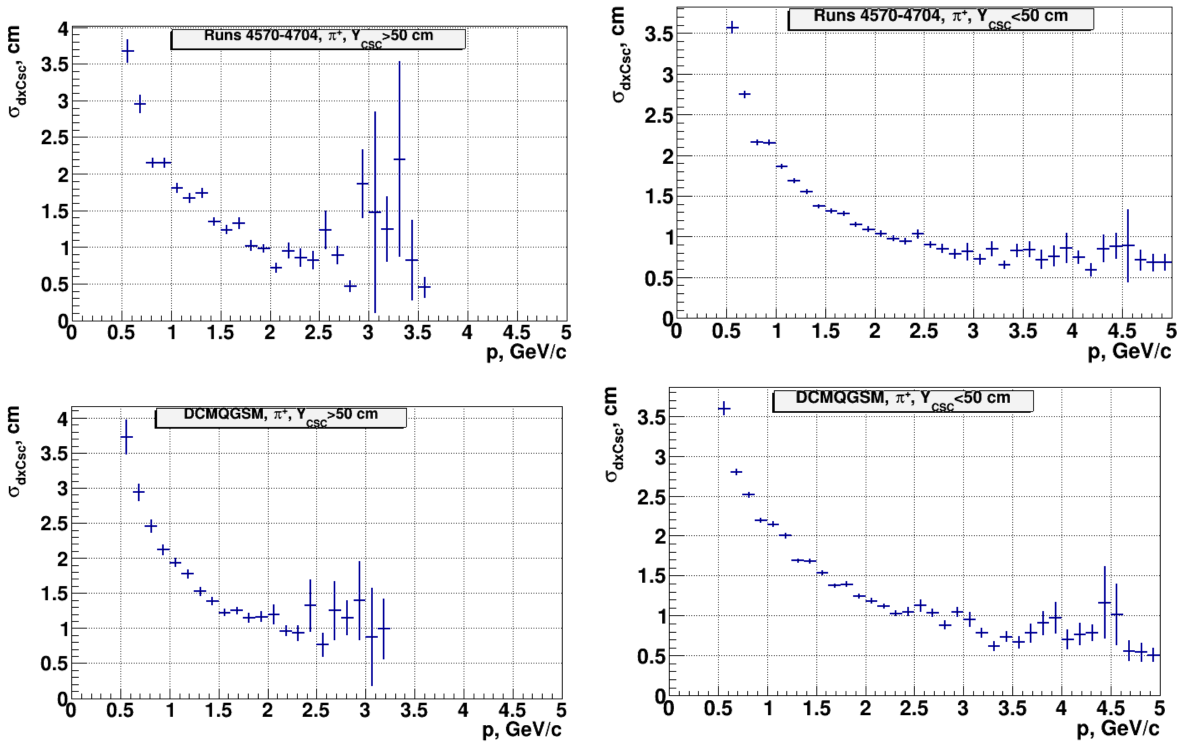

Fig. 6c. ToF-400 data and simulation: Sigma of residuals of CSC hits in the X projection with respect to reconstructed positive tracks in dependence on the particle momentum for two ranges in Y: upper plots - experimental data, lower plots – simulated tracks.

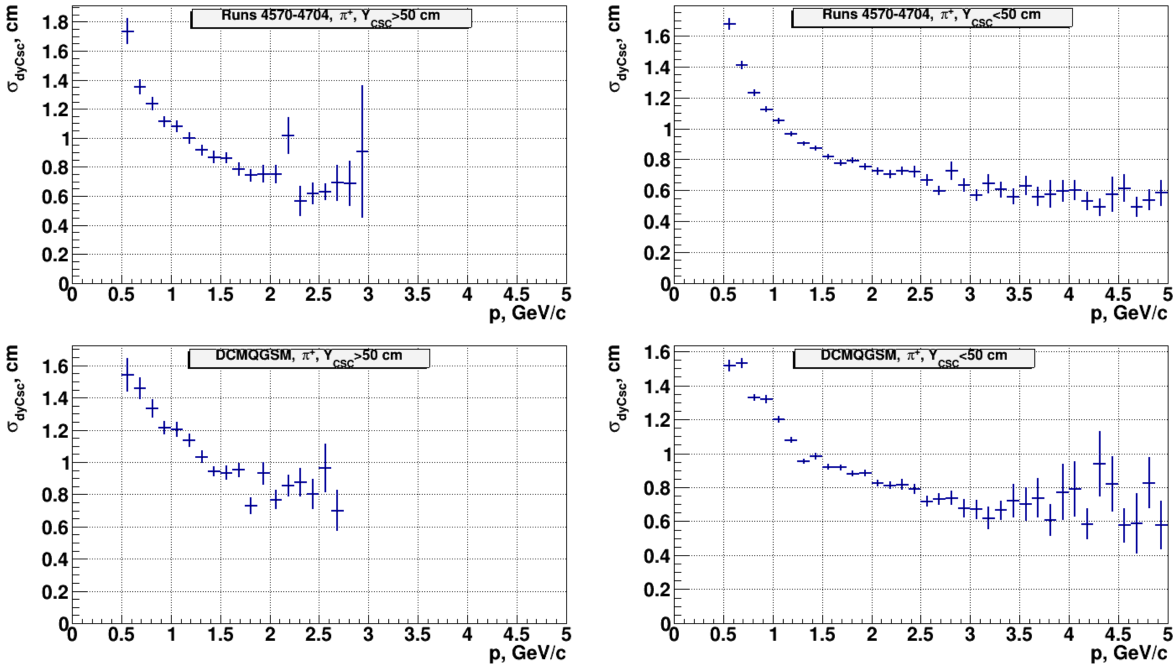

Fig. 6d. ToF-400 data and simulation: Sigma of residuals of CSC hits in the Y projection with respect to reconstructed positive tracks in dependence on the particle momentum for two ranges in Y: upper plots - experimental data, lower plots – simulated tracks.

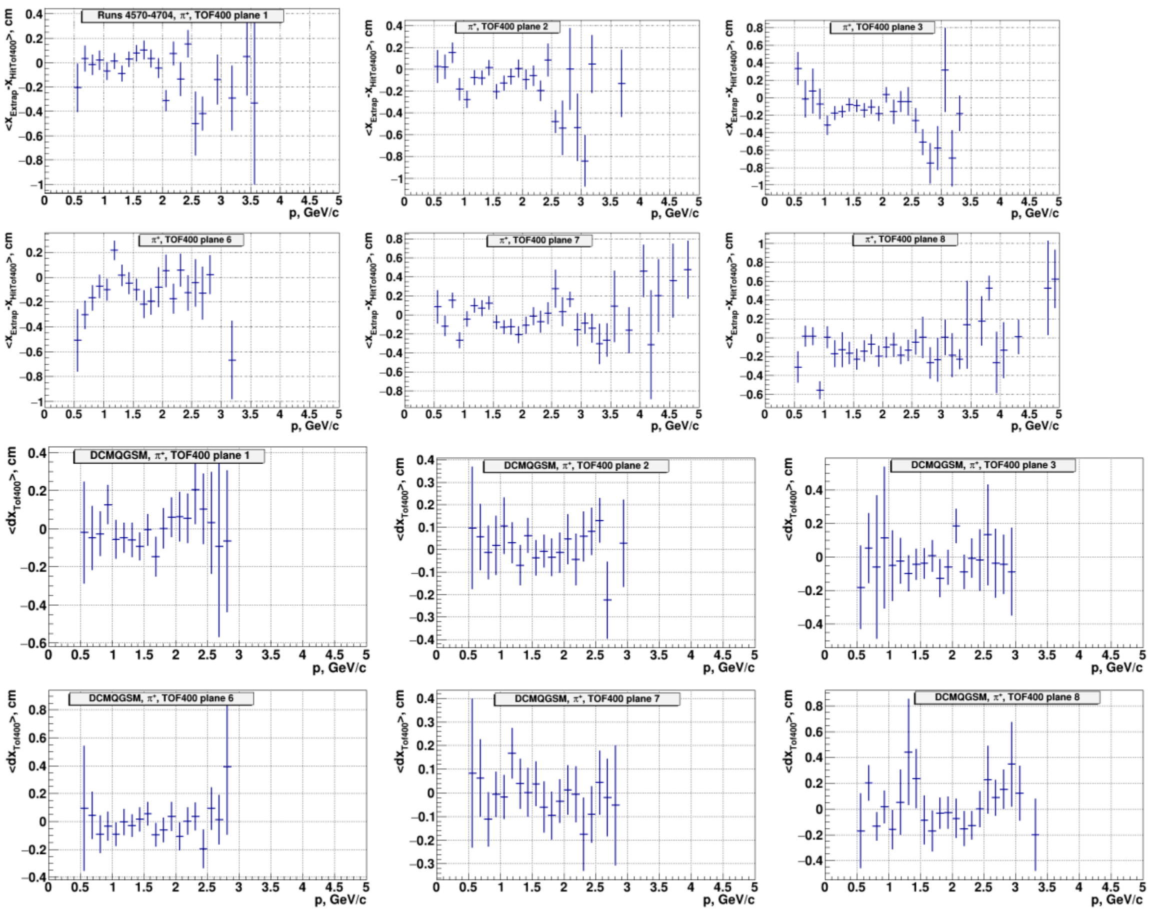

Fig. 7a. Mean values of residuals of ToF-400 hits in the X projection with respect to reconstructed positive tracks in dependence on the particle momentum: upper 6 plots - experimental data, lower 6 plots - simulated tracks.

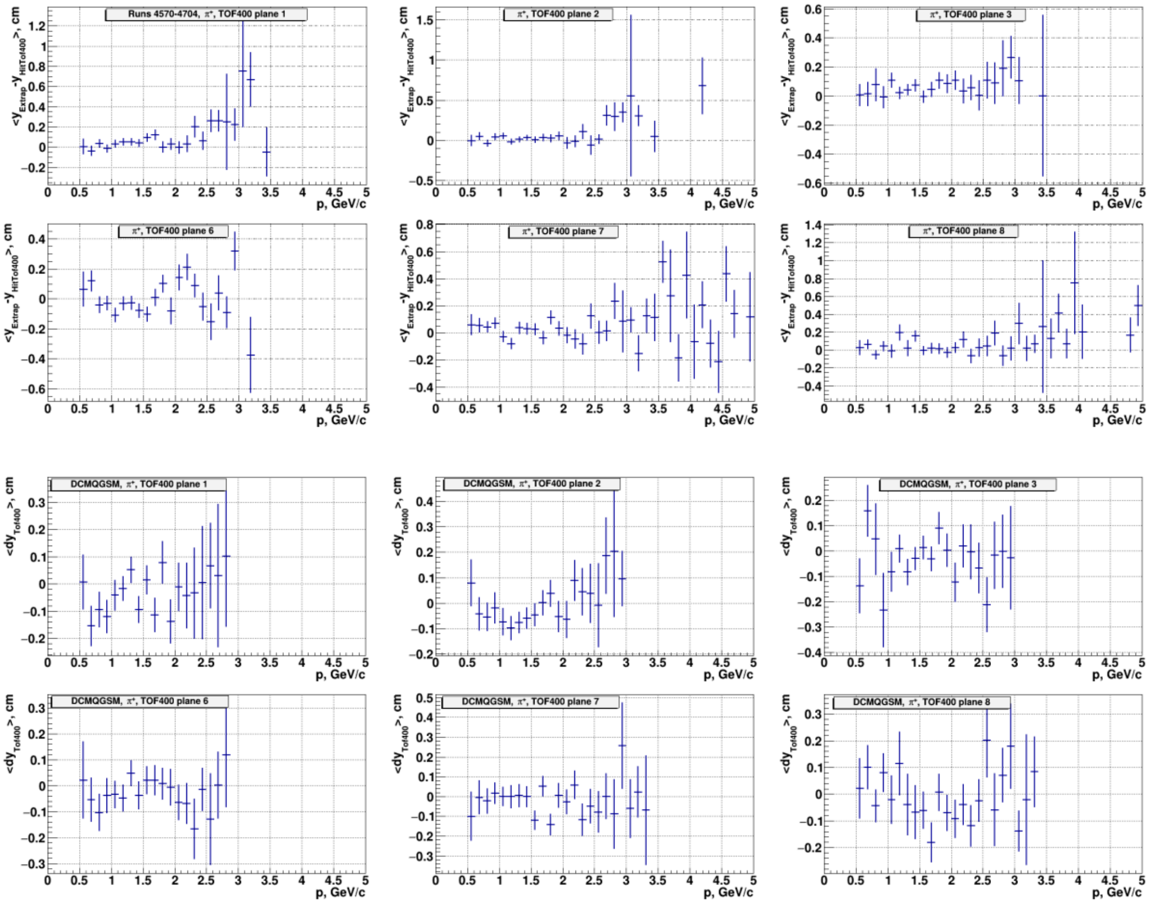

Fig. 7b. Mean values of residuals of ToF-400 hits in the Y projection with respect to reconstructed positive tracks in dependence on the particle momentum: upper 6 plots - experimental data, lower 6 plots - simulated tracks.

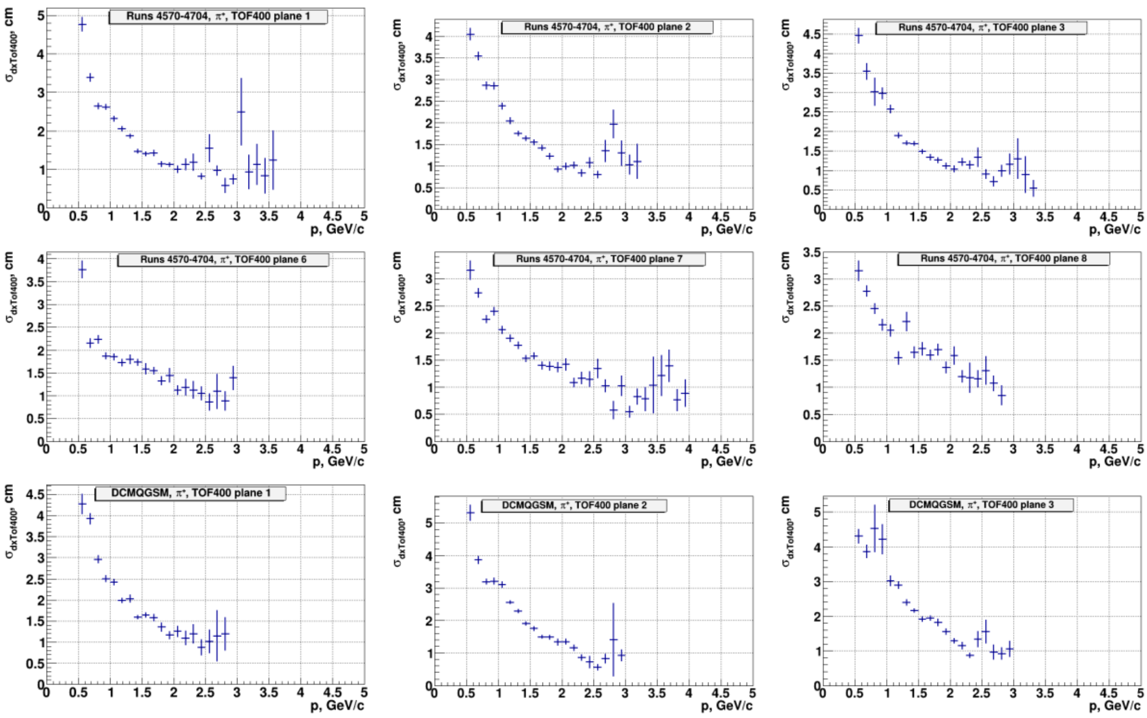

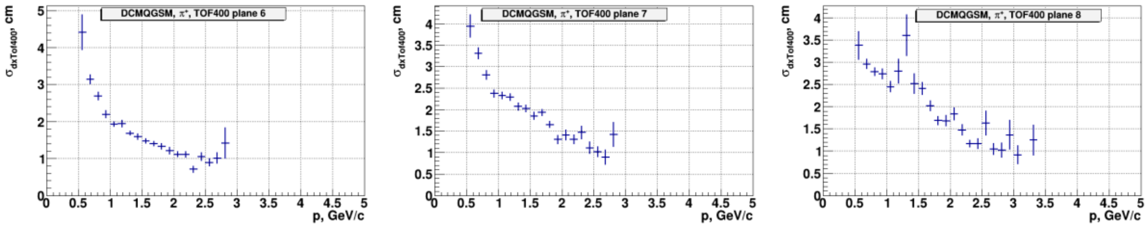

Fig. 7c. Sigma of residuals of ToF-400 hits in the X projection with respect to reconstructed positive tracks in dependence on the particle momentum: upper 6 plots - experimental data, lower 6 plots - simulated tracks.

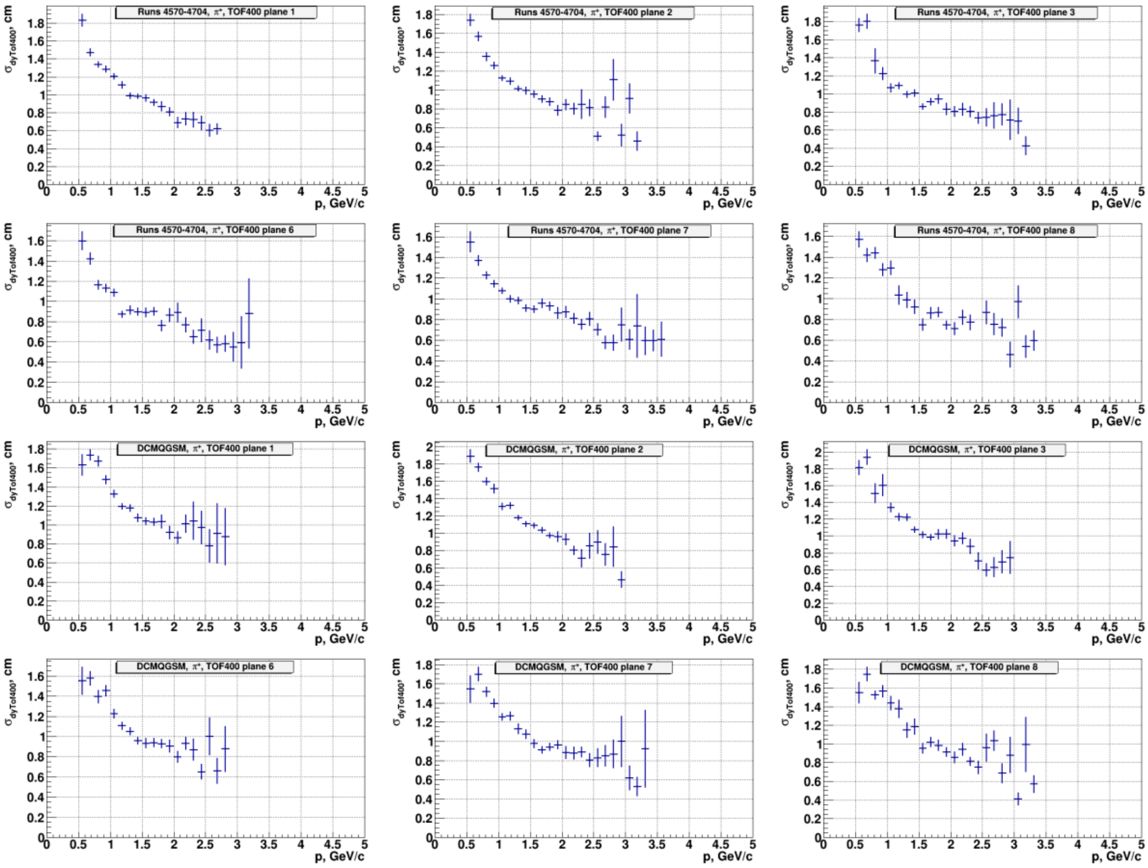

Fig. 7d. Sigma of residuals of ToF-400 hits in the Y projection with respect to reconstructed positive tracks in dependence on the particle momentum: upper 6 plots - experimental data, lower 6 plots - simulated tracks.

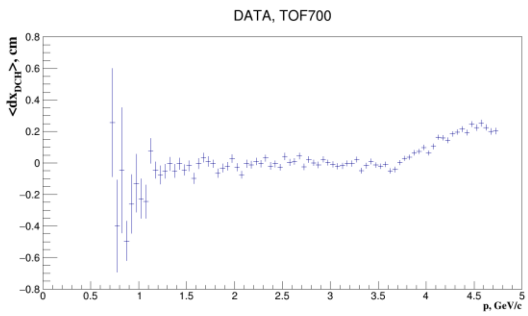

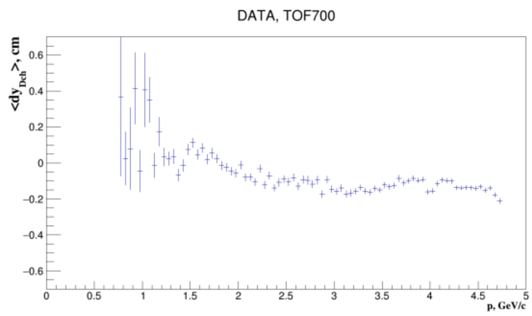

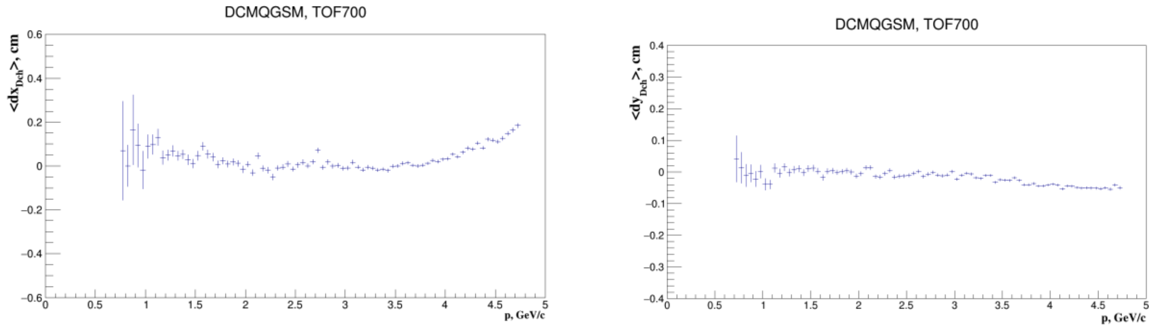

Fig. 8a. ToF-700 data and simulation: Mean values of residuals of DCH hits in X and Y projections with respect to reconstructed positive tracks in dependence on the particle momentum: upper plots experimental data, lower plots – simulated tracks.

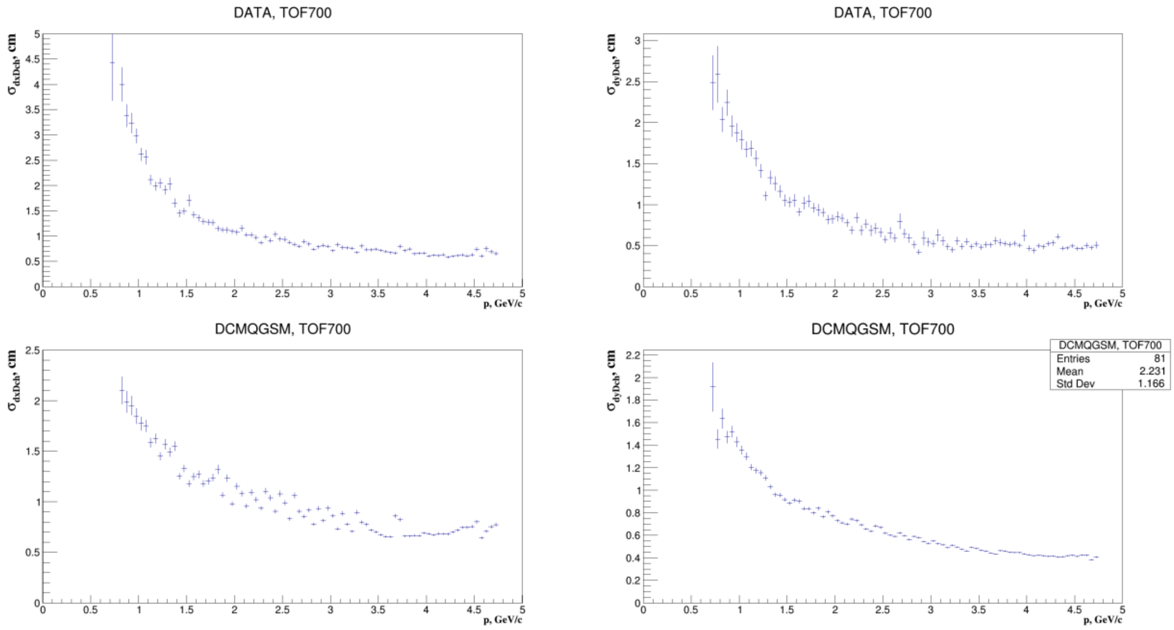

Fig. 8b. ToF-700 data and simulation: Sigma of residuals of DCH hits in the X and Y projections with respect to reconstructed positive tracks in dependence on the particle momentum: upper plots - experimental data, lower plots – simulated tracks.

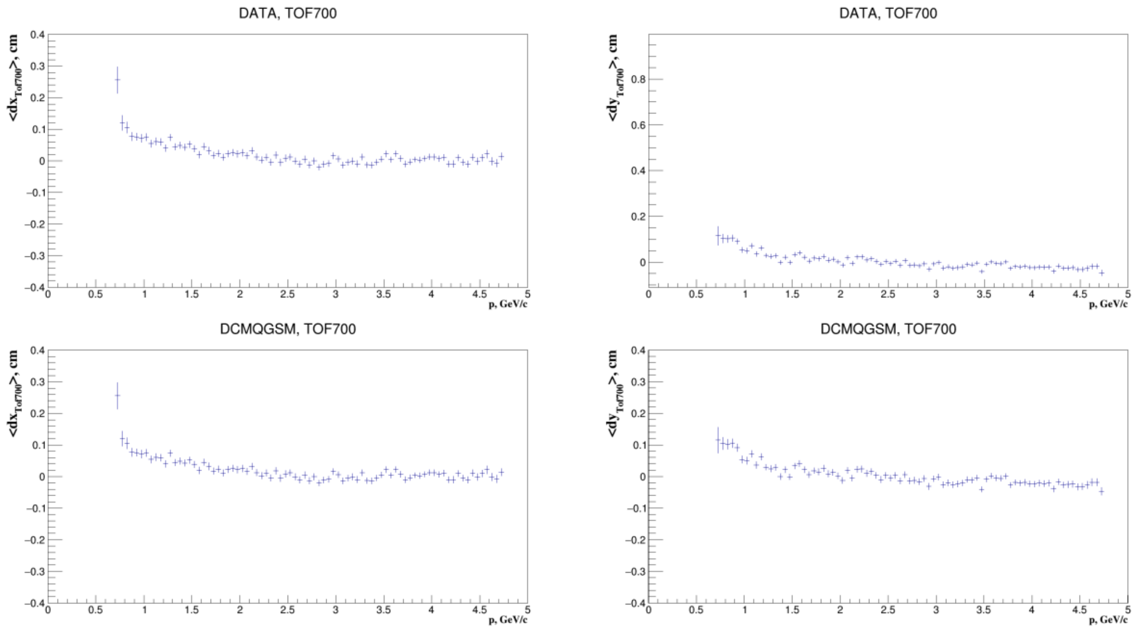

Fig. 9a. Mean values of residuals of ToF-700 hits in the X and Y projections with respect to

reconstructed positive tracks in dependence on the particle momentum: upper plots - experimental data, lower plots - simulated tracks.

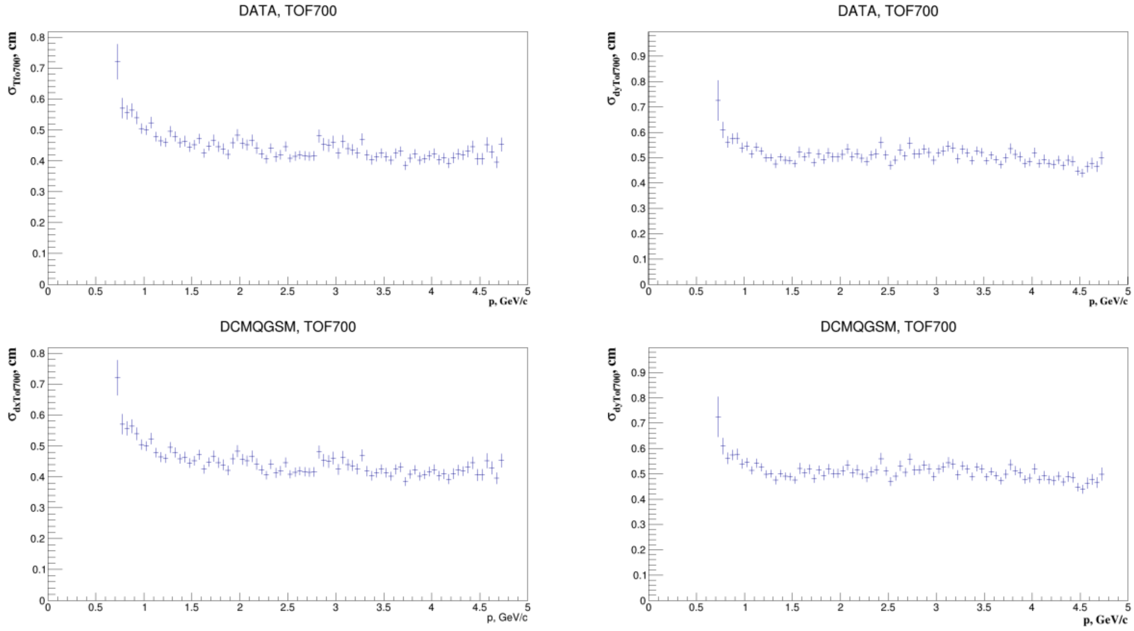

Fig. 9b. Sigma of residuals of ToF-700 hits in the X and Y projections with respect to reconstructed positive tracks in dependence on the particle momentum: upper plots - experimental data, lower plots - simulated tracks.

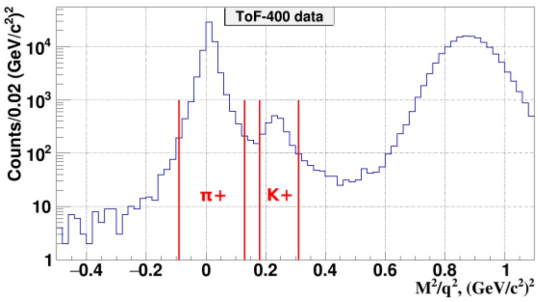

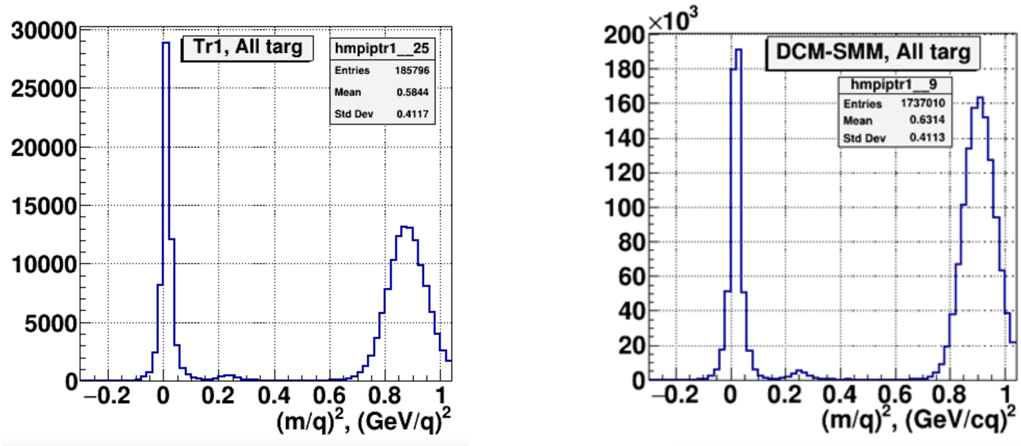

Fig. 10a. Spectrum of mass squared of particles identified in ToF-400 in *Ar+A* interactions at 3.2 AGeV argon beam energy: left) experimental events, right) simulated events.

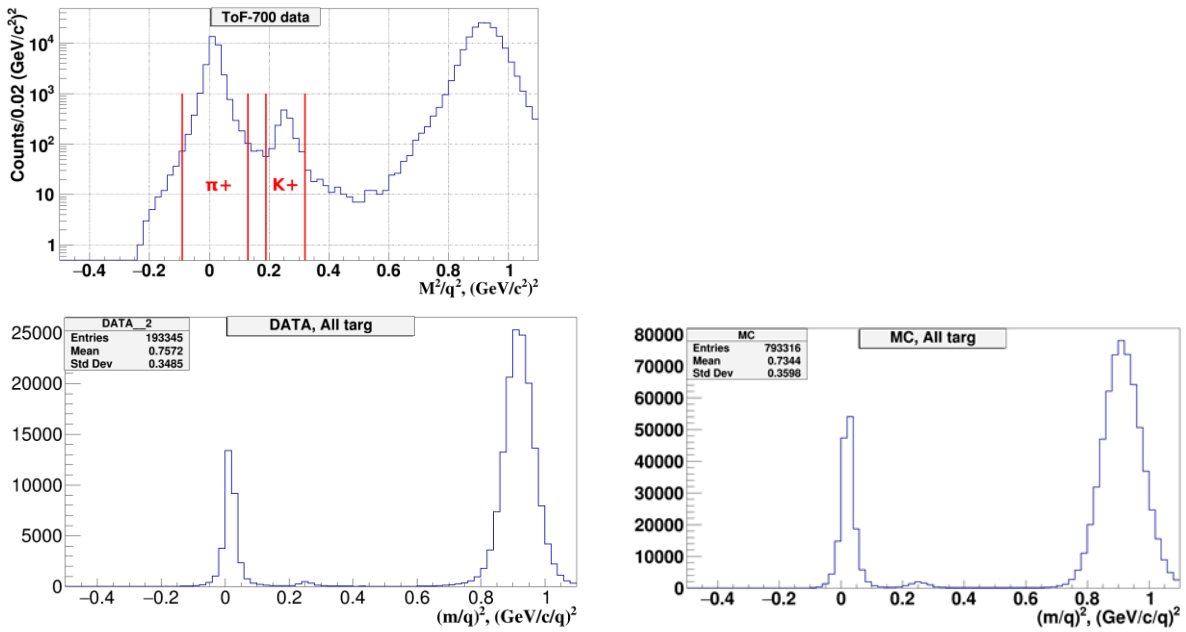

Fig. 10b. Spectrum of mass squared of particles identified in ToF-700 in Ar+A interactions at 3.2 AGeV argon beam energy: left) experimental events, right) simulated events.

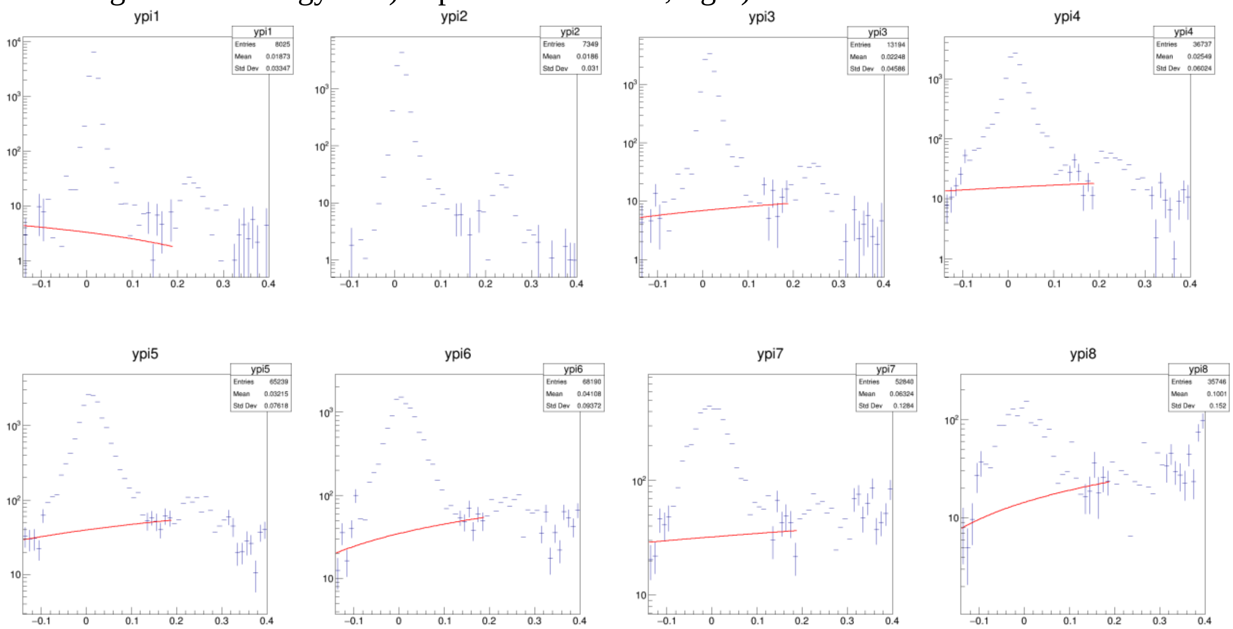

Fig. 10c. Spectrum of mass squared in bins of y of π+ identified in ToF-400 in Ar+Cu interactions: background subtraction by the linear fit described in the text.

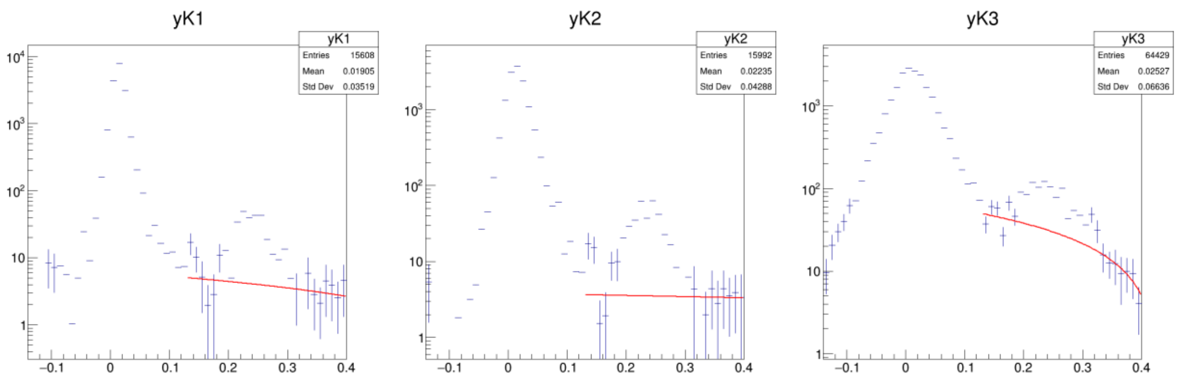

Fig. 10d. Spectrum of mass squared in bins of y of K+ identified in ToF-400 in Ar+Cu interactions: background subtraction by the linear fit described in the text.

.

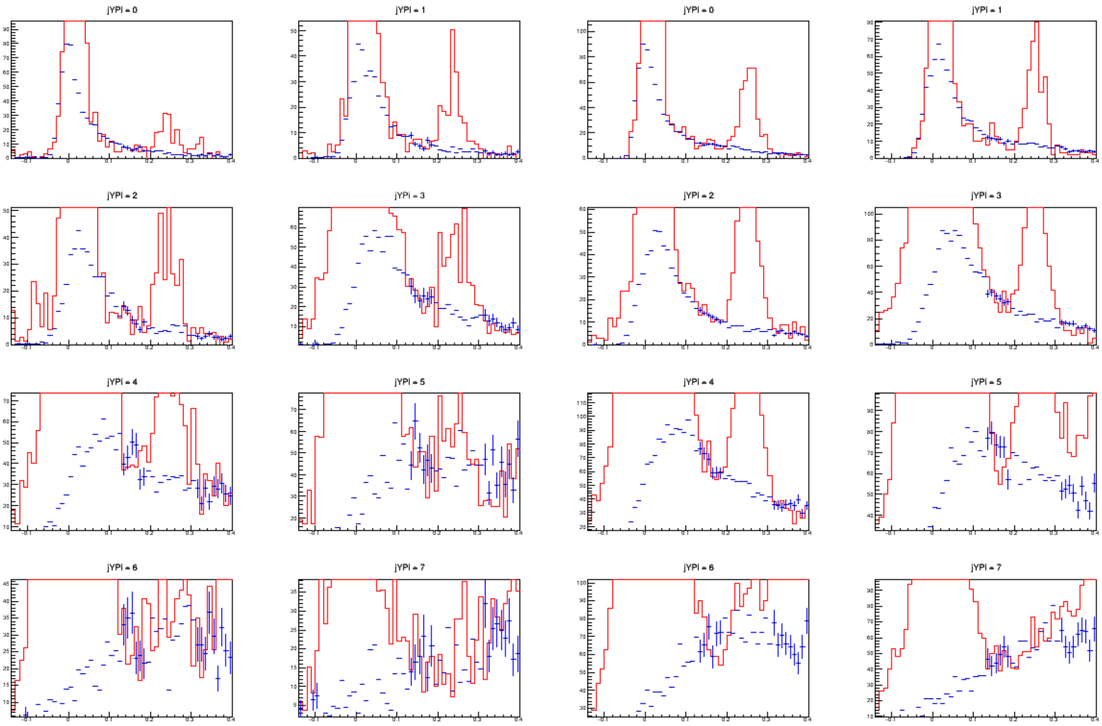

Fig. 10e. Spectrum of mass squared in bins of y of π+ identified in ToF-400 in Ar+Sn interactions at 3.2 AGeV argon beam energy: left) experimental events, right) simulated events. Background (blue histogram) is taken from mixed events and normalized to the red signal histogram in the mass squared range between the π+ and K+ peaks.

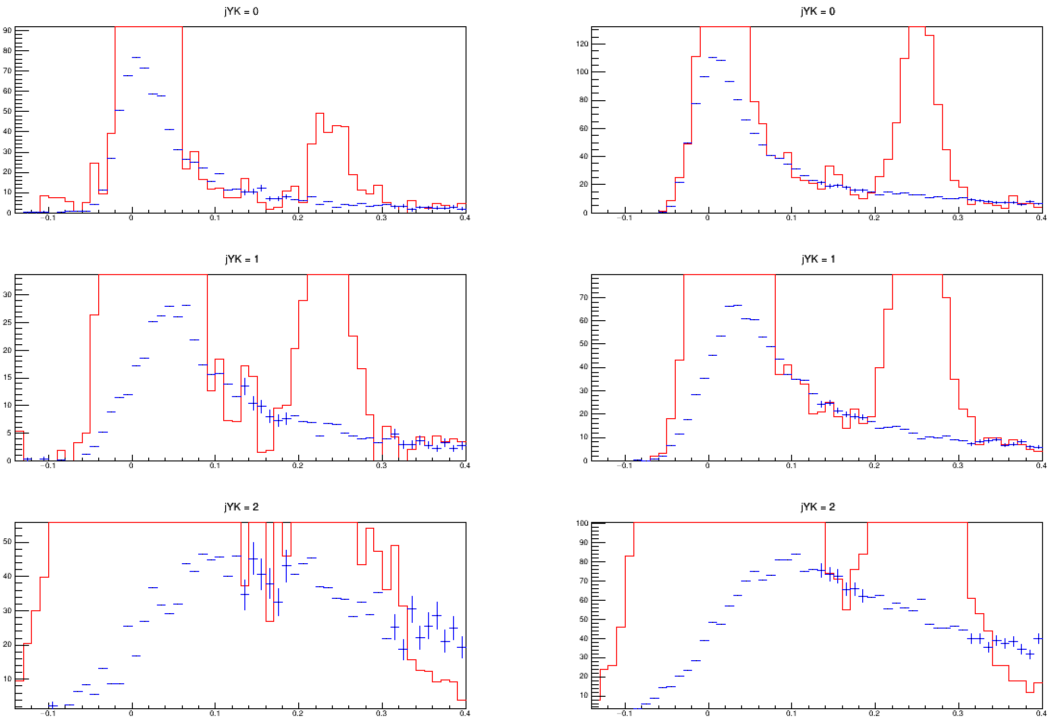

Fig. 10f. Spectrum of mass squared in bins of y of K+ identified in ToF-400 in Ar+Sn interactions: left) experimental events, right) simulated events. Background (blue histogram) is taken from mixed events and normalized to the red signal histogram in the mass squared range below and above the K+ peak.

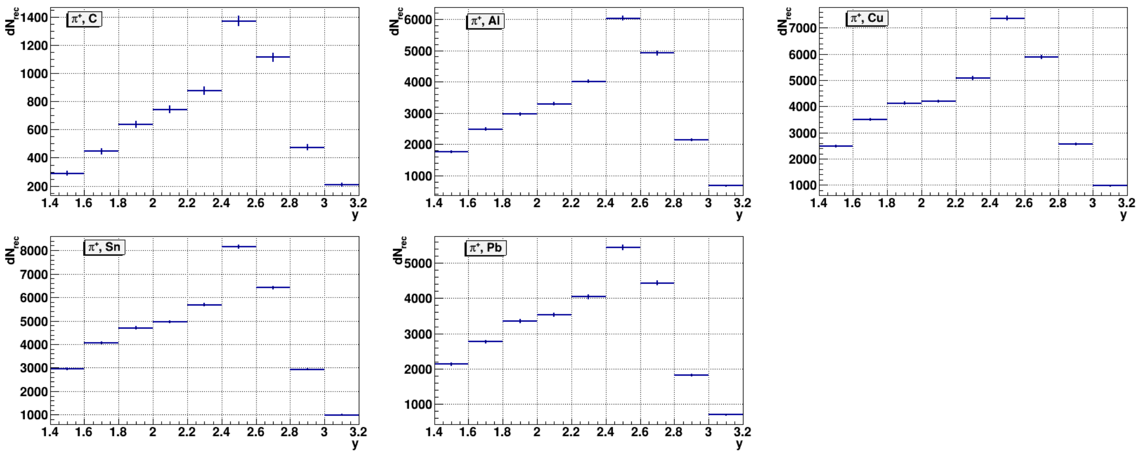

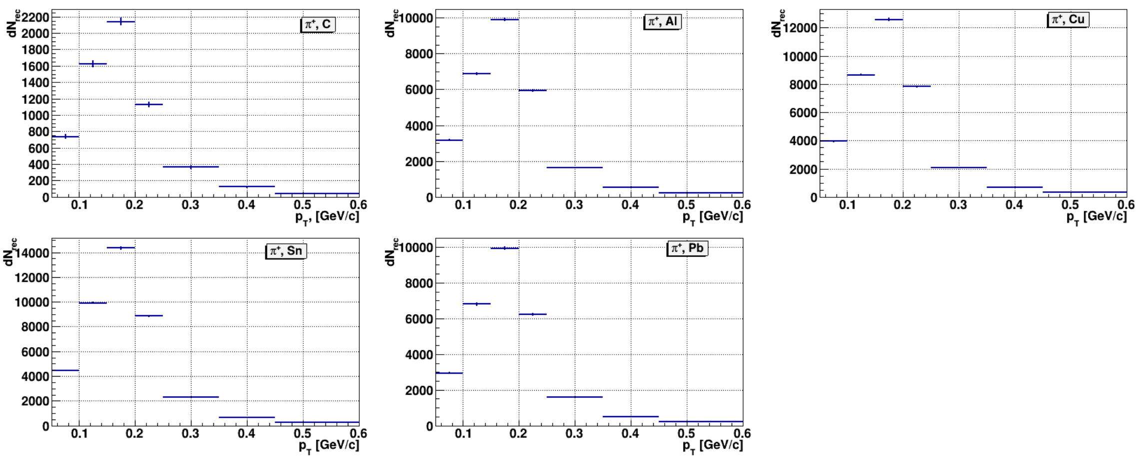

Fig.11a. Number of reconstructed π^+ in ToF-400 in interactions of 3.2 AGeV argon beam with *C, Al, Cu, Sn, Pb* targets in bins of y_{lab} (upper plots) and p_T (lower plots).

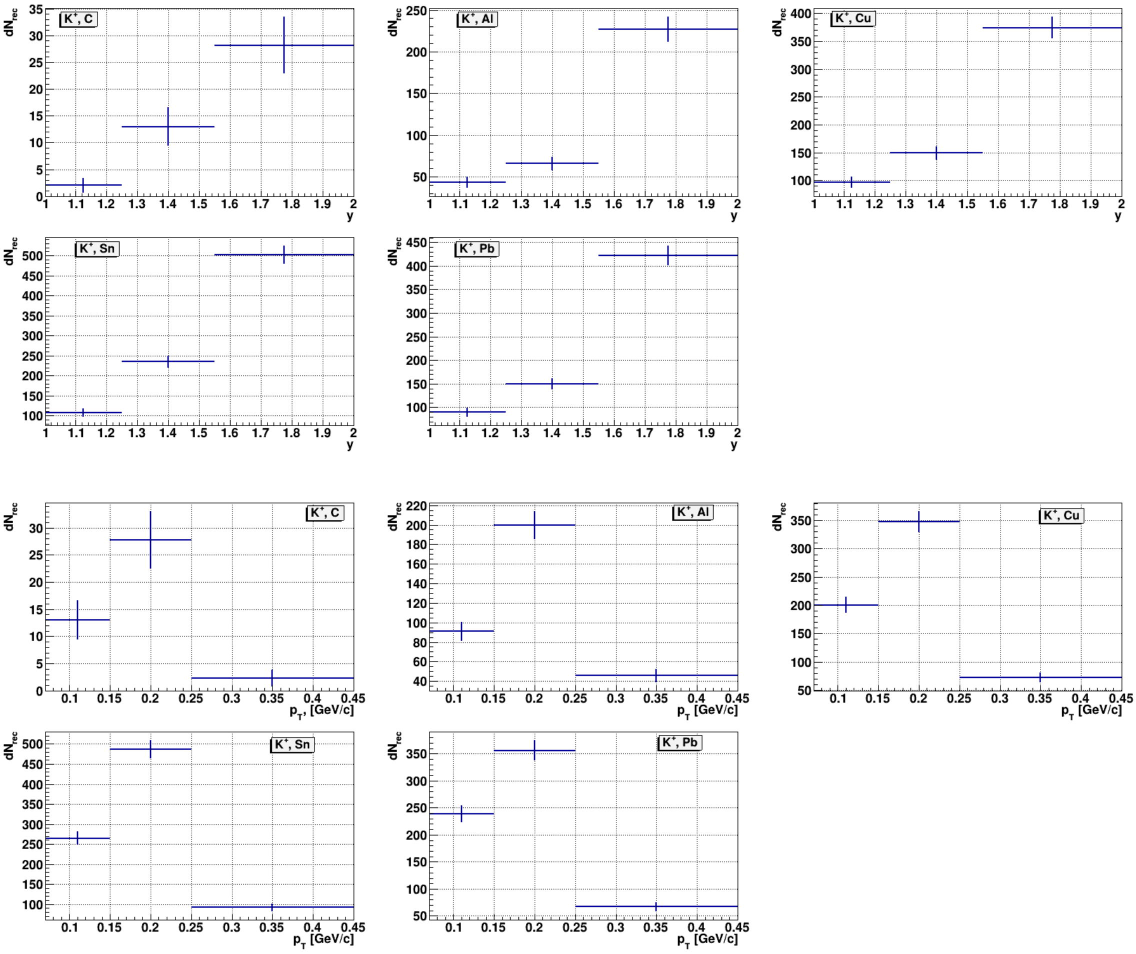

Fig.11b. Number of reconstructed K^+ in ToF-400 in interactions of 3.2 AGeV argon beam with *C, Al, Cu, Sn, Pb* targets in bins of y_{lab} (upper plots) and p_T (lower plots).

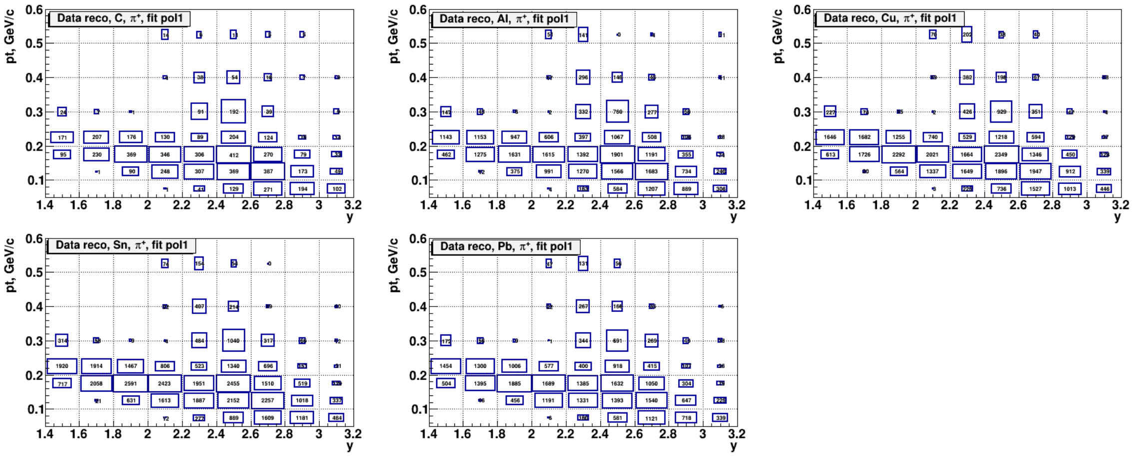

Fig.11c. Number of reconstructed π^+ in ToF-400 in interactions of 3.2 AGeV argon beam with *C, Al, Cu, Sn, Pb* targets in bins of (y_{lab}, p_T).

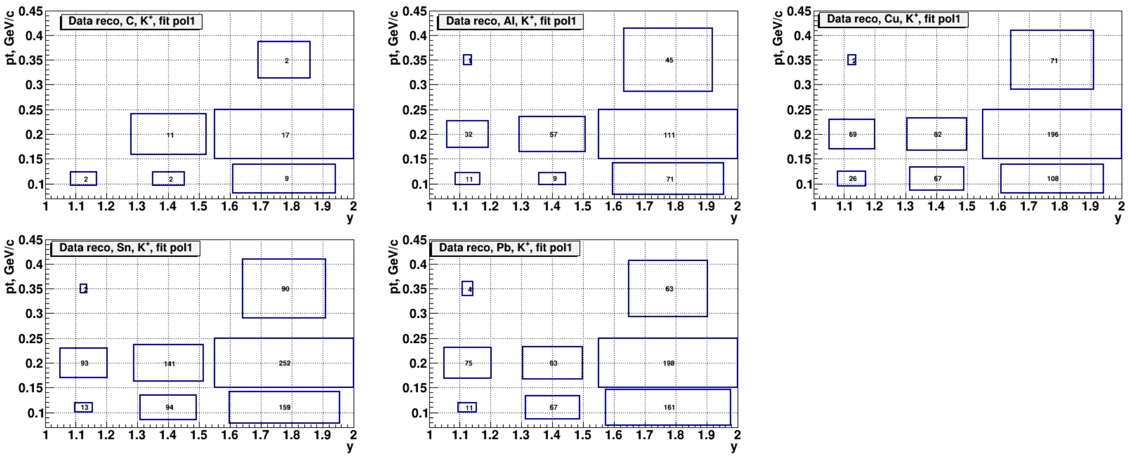

Fig.11d. Number of reconstructed K^{+} in ToF-400 in interactions of 3.2 AGeV argon beam with *C, Al, Cu, Sn, Pb* targets in bins of (y_{lab}, p_T).

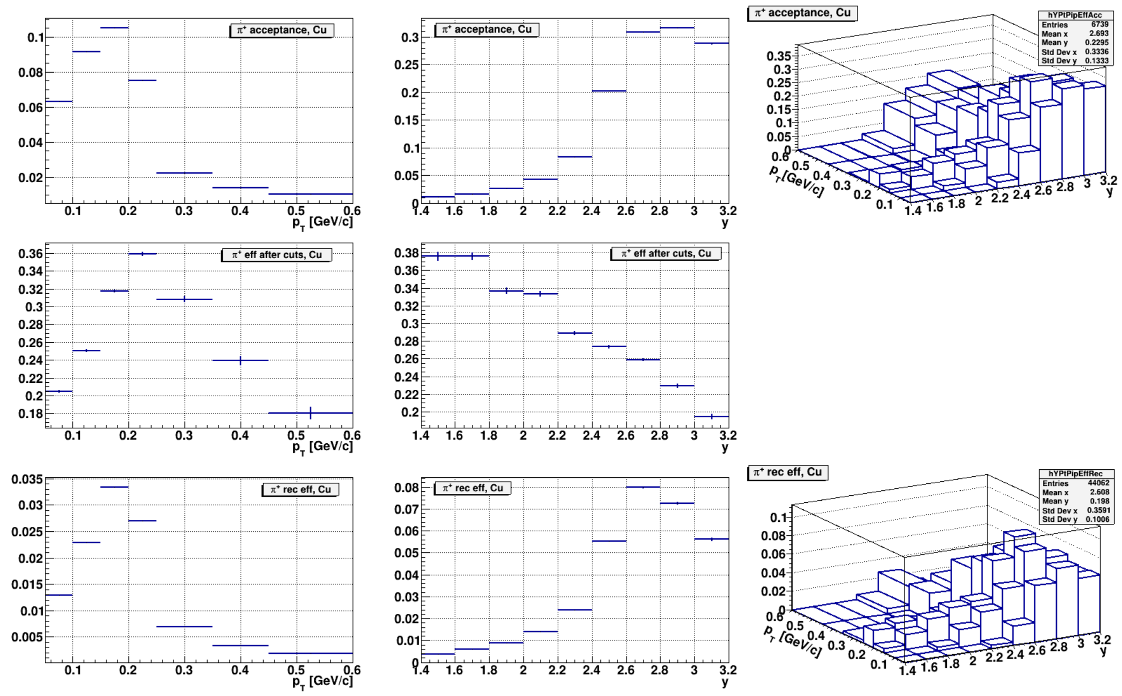

Fig.12a. π+ geometrical acceptance (upper plots); efficiency of reconstruction of accepted π+ after applying kinematic and spatial cuts (middle plots) and full reconstruction efficiency (lower plots) shown in bins of rapidity y_{lab} in the laboratory system, transverse momentum p_T and (y,p_T). Results are shown for Ar+Cu interactions at 3.2 AGeV argon beam energy.

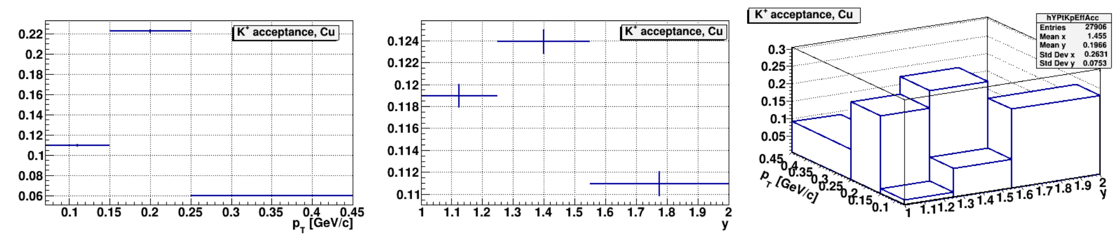

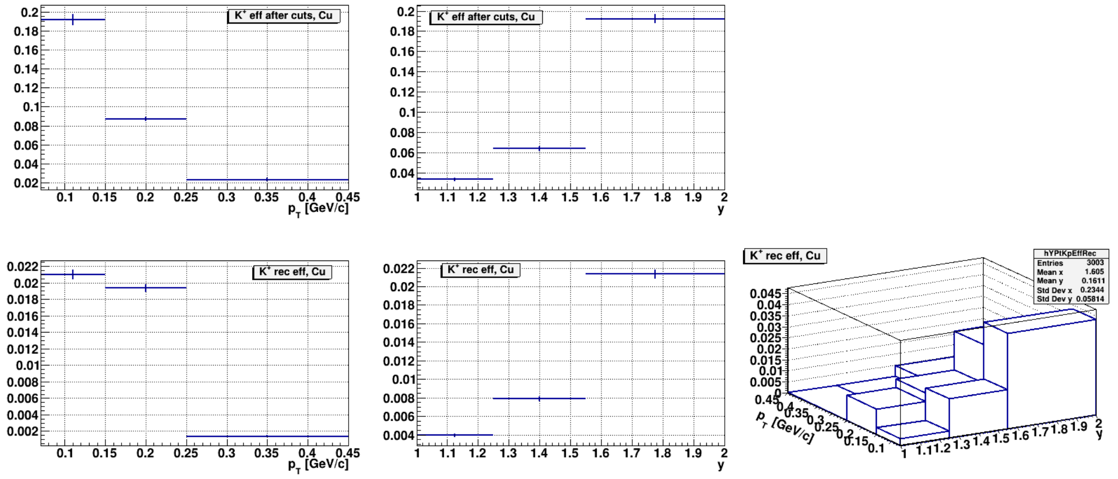

Fig.12b. K+ geometrical acceptance (upper plots); efficiency of reconstruction of accepted K+ after applying kinematic and spatial cuts (middle plots) and full reconstruction efficiency (lower plots) shown in bins of rapidity y_{lab} in the laboratory system, transverse momentum p_T and (y,p_T). Results are shown for Ar+Cu interactions at 3.2 AGeV argon beam energy.

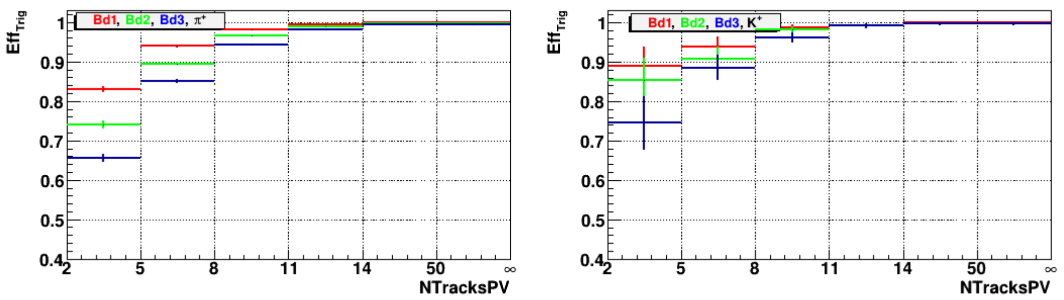

Fig.13a. Dependence of the BD trigger efficiency on the number of tracks from the primary vertex calculated in events with π^+ (left plot) and K+ (right plot) produced in interactions of the argon beam with the *C*, *Al*, *Cu*, *Sn*, *Pb* targets.

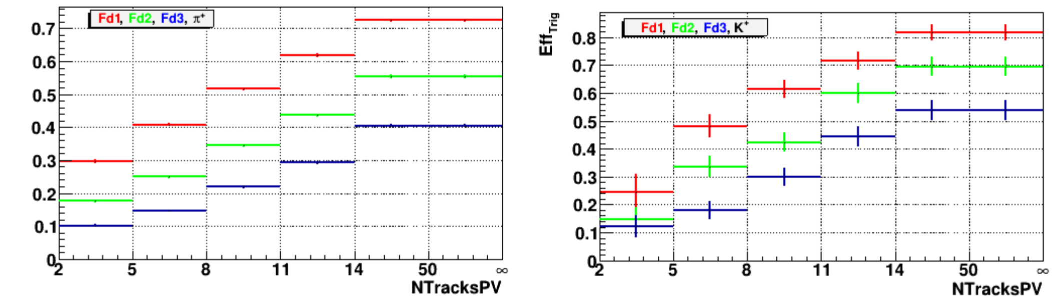

Fig.13b. Dependence of the FD trigger efficiency on the number of tracks from the primary vertex calculated in events with π^+ (left plot) and K+ (right plot) produced in interactions of the argon beam with the *C*, *Al*, *Cu*, *Sn*, *Pb* targets.

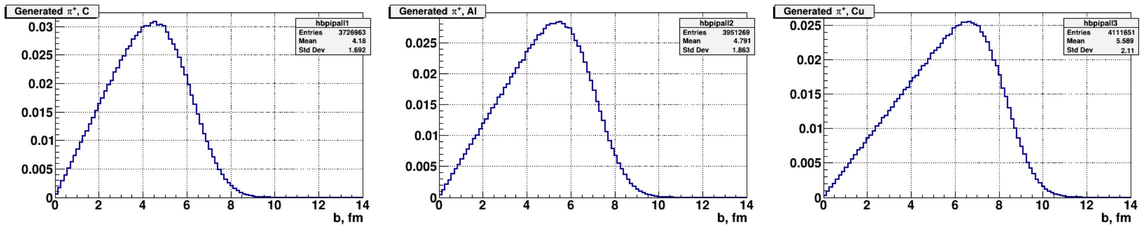

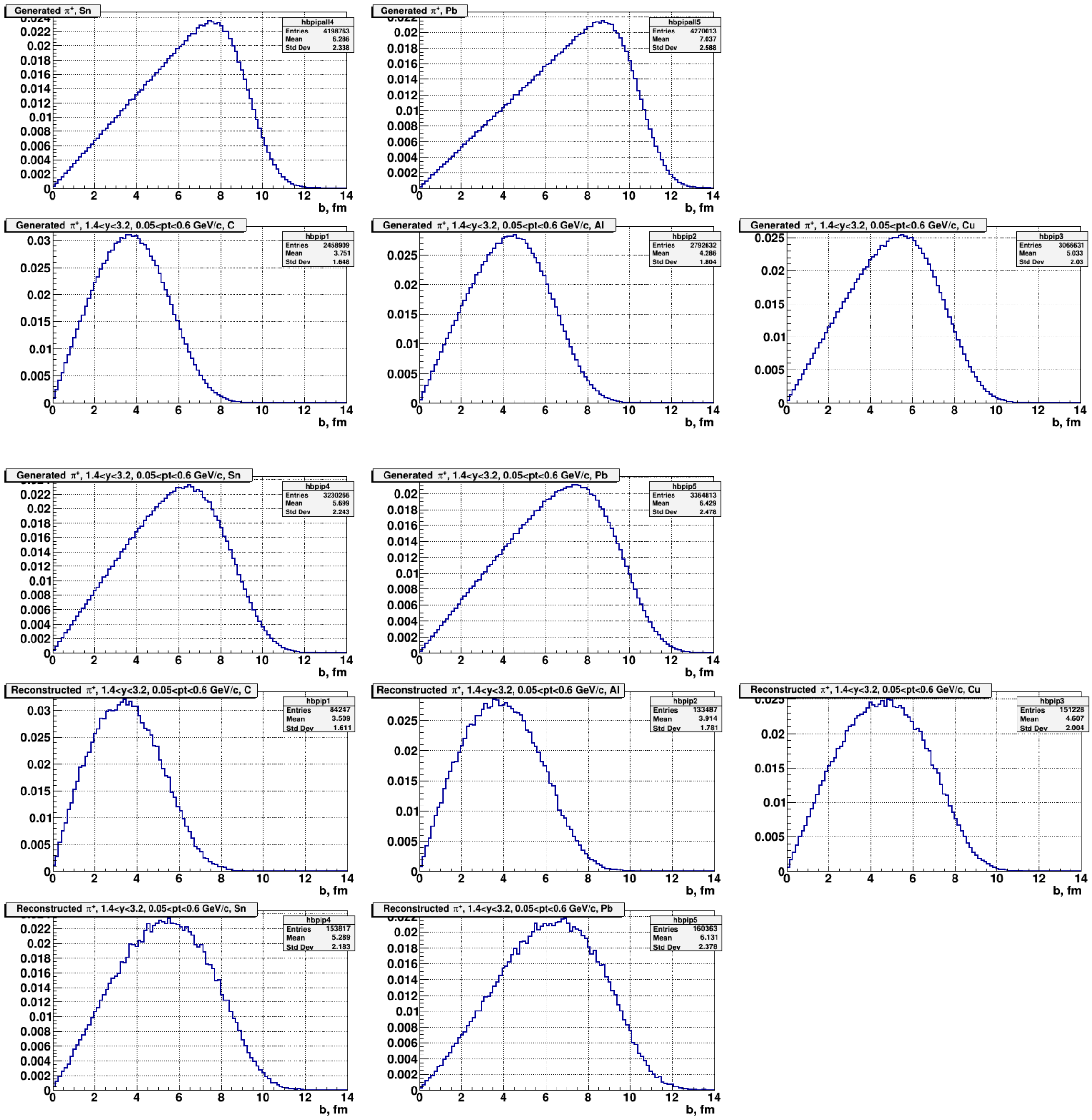

Fig. 14a. Impact parameter distributions of minimum bias interactions of 3.2 AGeV argon beam with C, Al, Cu, Pb targets, with $\pi+$ generated with the DCM-SMM model in the full kinematical range (upper plots). Impact parameter distribution of minimum bias events with $\pi+$ generated with the DCM-SMM model in the kinematical range of the BM@N measurement (middle plots). Impact parameter distribution of DCM-SMM minimum bias events with reconstructed π^+ (lower plots).

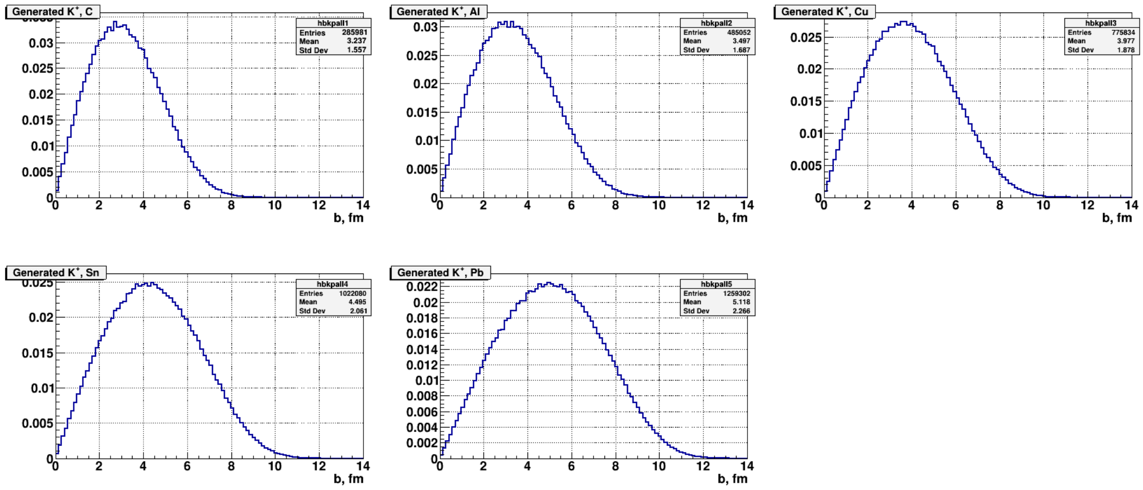

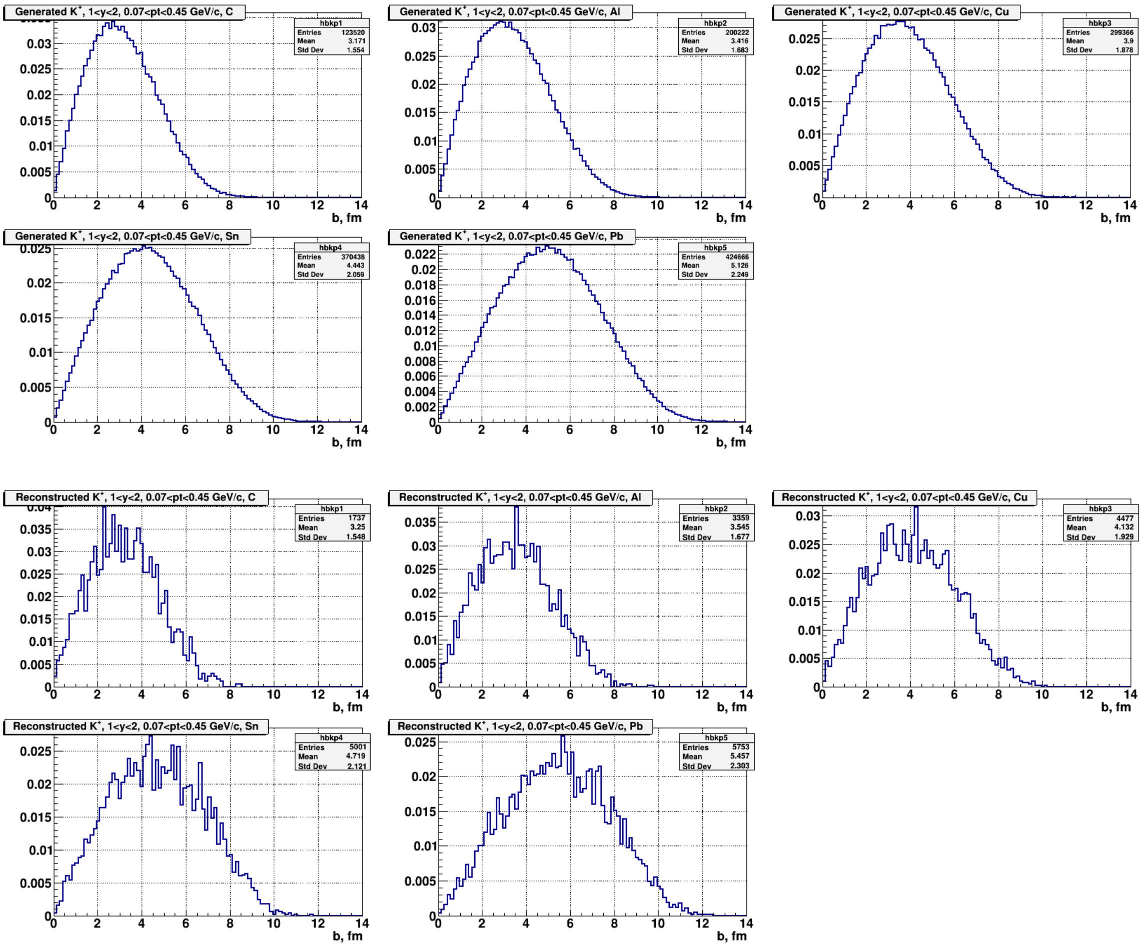

Fig. 14b. Impact parameter distributions of minimum bias interactions of 3.2 AGeV argon beam with C, Al, Cu, Pb targets, with *K+* generated with the DCM-SMM model in the full kinematical range (upper plots). Impact parameter distribution of minimum bias events with *K+* generated with the DCM-SMM model in the kinematical range of the BM@N measurement (middle plots). Impact parameter distribution of DCM-SMM minimum bias events with reconstructed K^+ (lower plots).

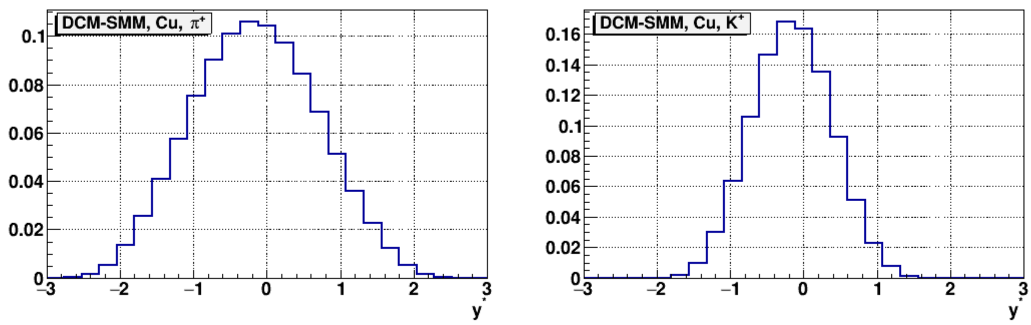

Fig.14c. Rapidity spectra of π^+ (left plot) and K+ (right plot) in minimum bias interactions of the 3.2 AGeV argon beam with the Cu target, generated with the DCM-SMM model.

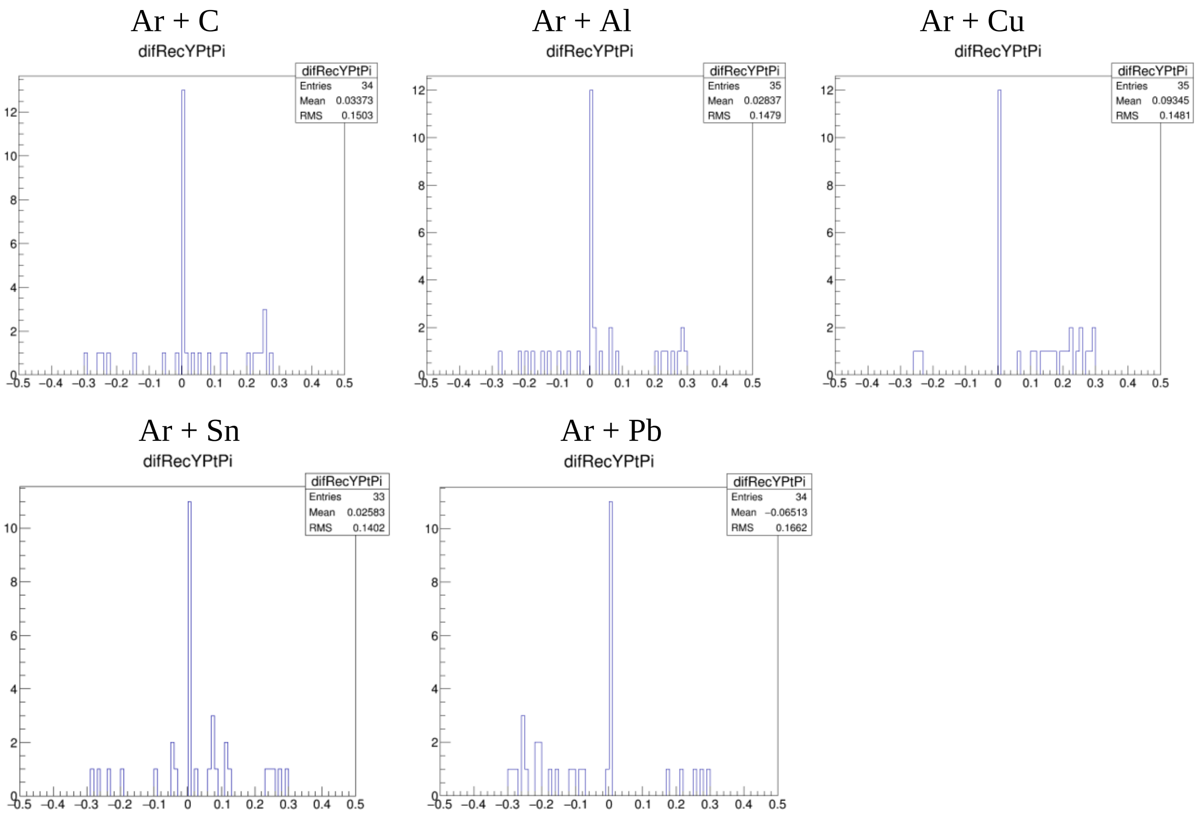

Fig.14d. Relative difference of π+ yields measured in *(y,p_T)* bins using ToF-400 and ToF-700 data in Ar + C, Al, Cu, Sn, Pb interactions.

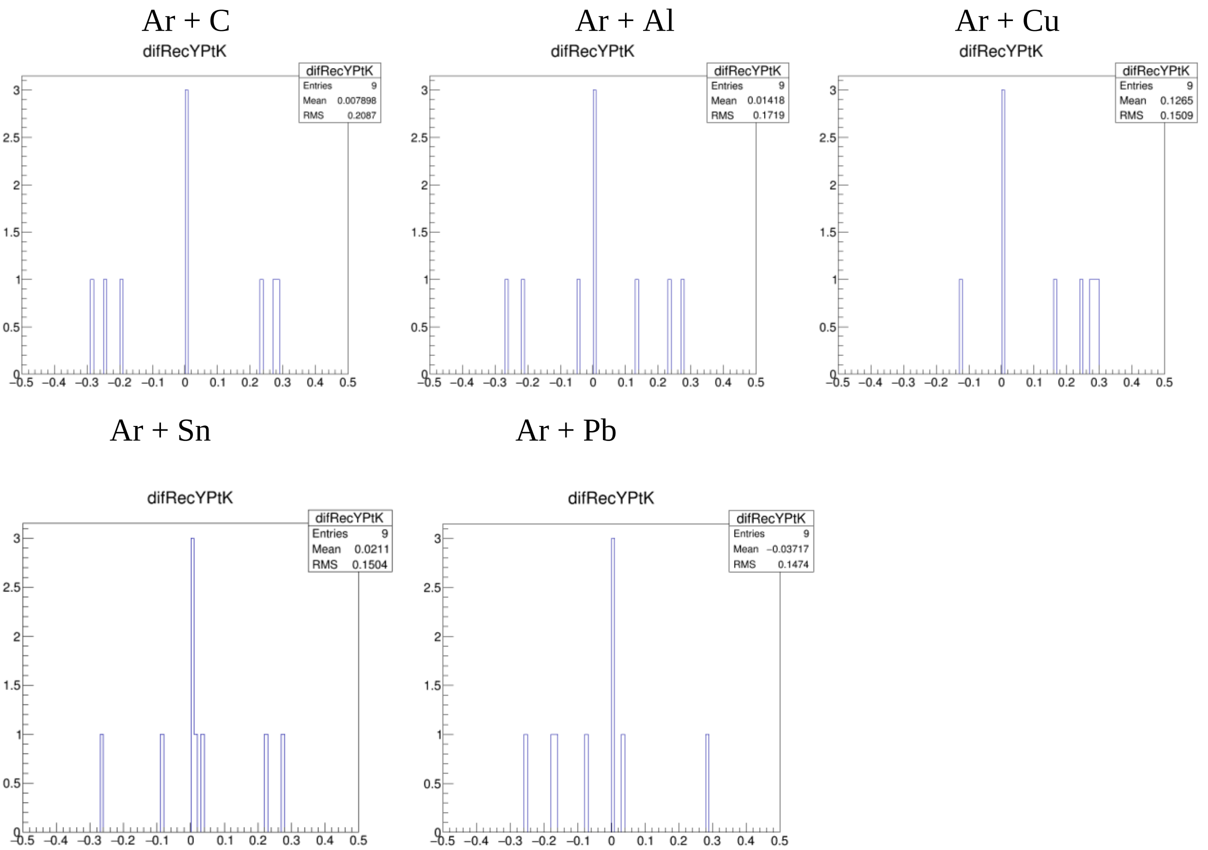

Fig.14e. Relative difference of K+ yields measured in 9 *(y,p_T)* bins using ToF-400 and ToF-700 data in Ar + C, Al, Cu, Sn, Pb interactions.

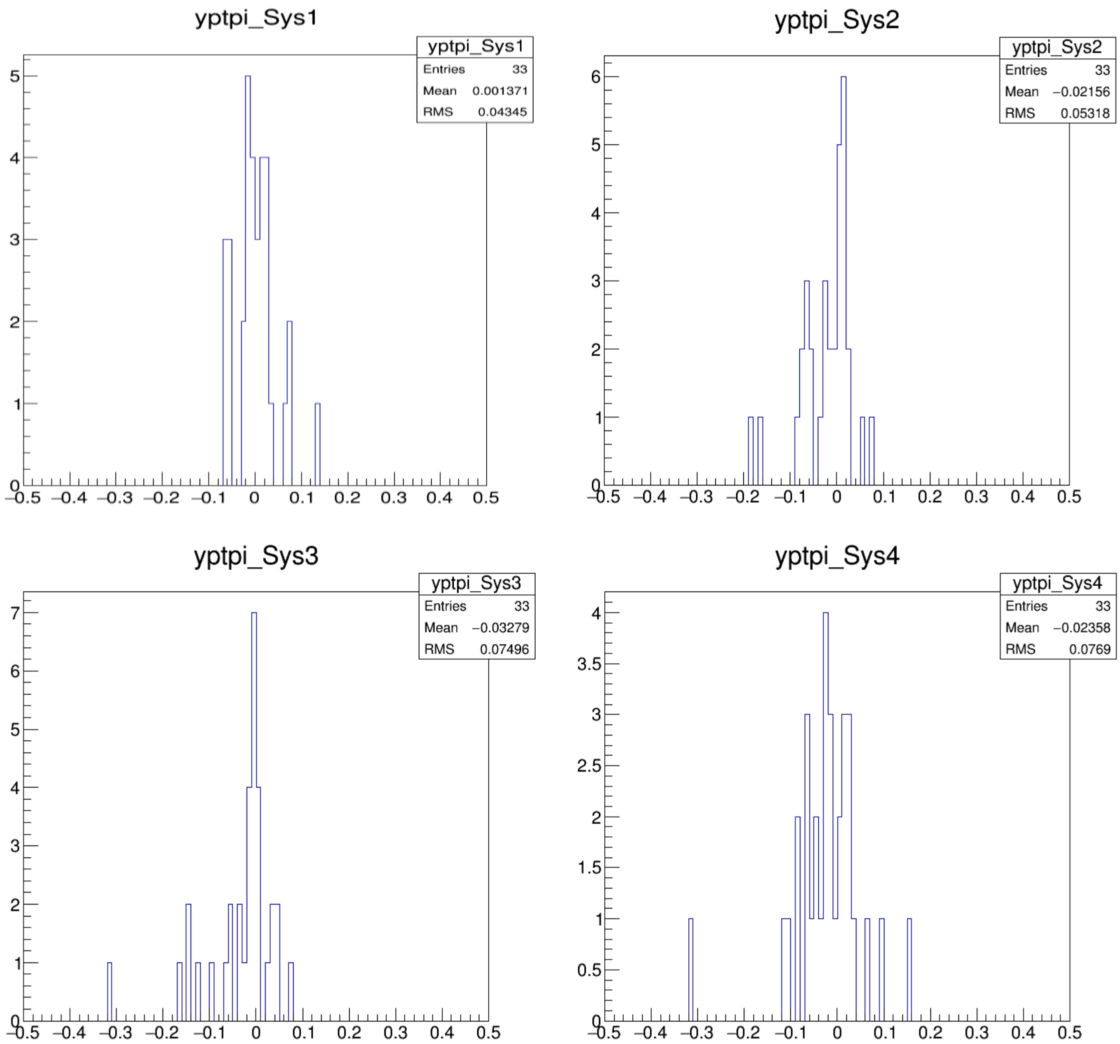

Fig.14f. Relative difference of π+ yields in *(y,p$_T$)* bins, originated from different sources of systematic uncertainties in Ar + Sn data: Sys1 – trigger efficiency in dependence on the vertex track multiplicity and vertex position, Sys2 – X,Y vertex distribution in Data vs MC, Sys3 – method of K+ background subtraction (linear fit instead of "mixed event" method), Sys4 – data based BD trigger vs all BD+FD data.

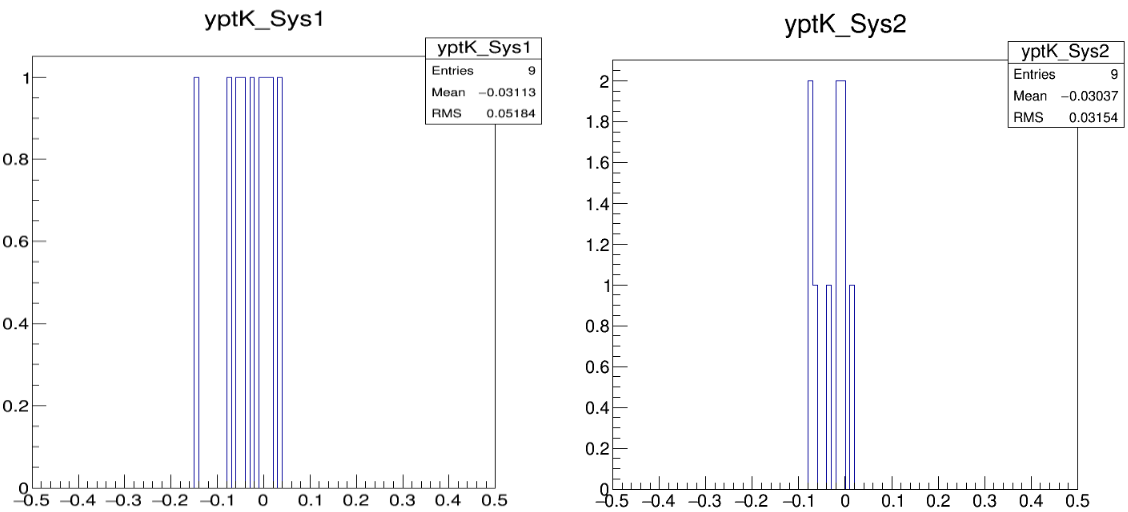

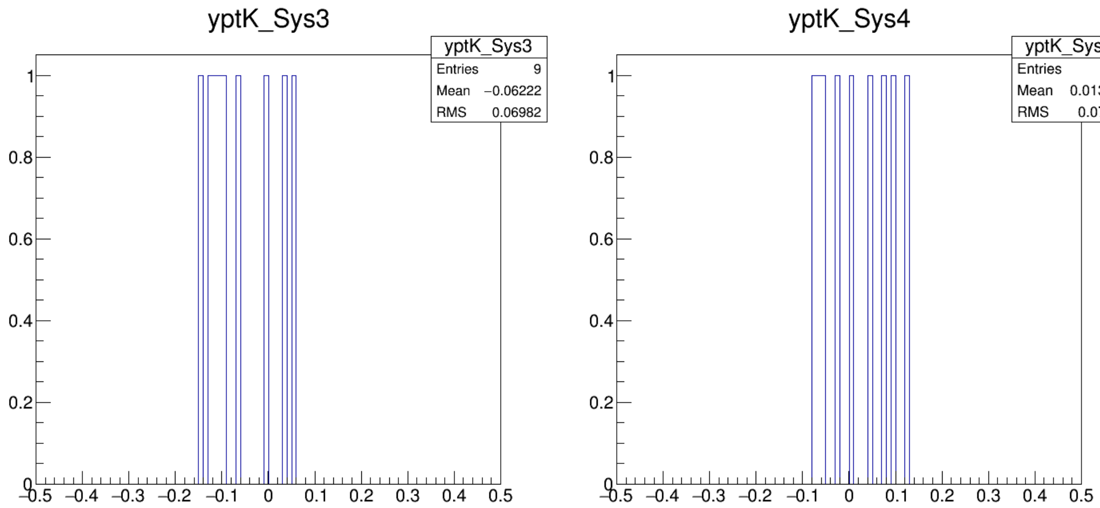

Fig.14i. Relative difference of K+ yields in 9 *(y,p_T)* bins, originated from different sources of systematic uncertainties in Ar + Sn data: Sys1 – trigger efficiency in dependence on the vertex track multiplicity and vertex position,, Sys2 – X,Y vertex distribution, Sys3 – method of K+ background subtraction (linear fit instead of "mixed event" method), Sys4 – data based BD trigger vs all BD+FD data.

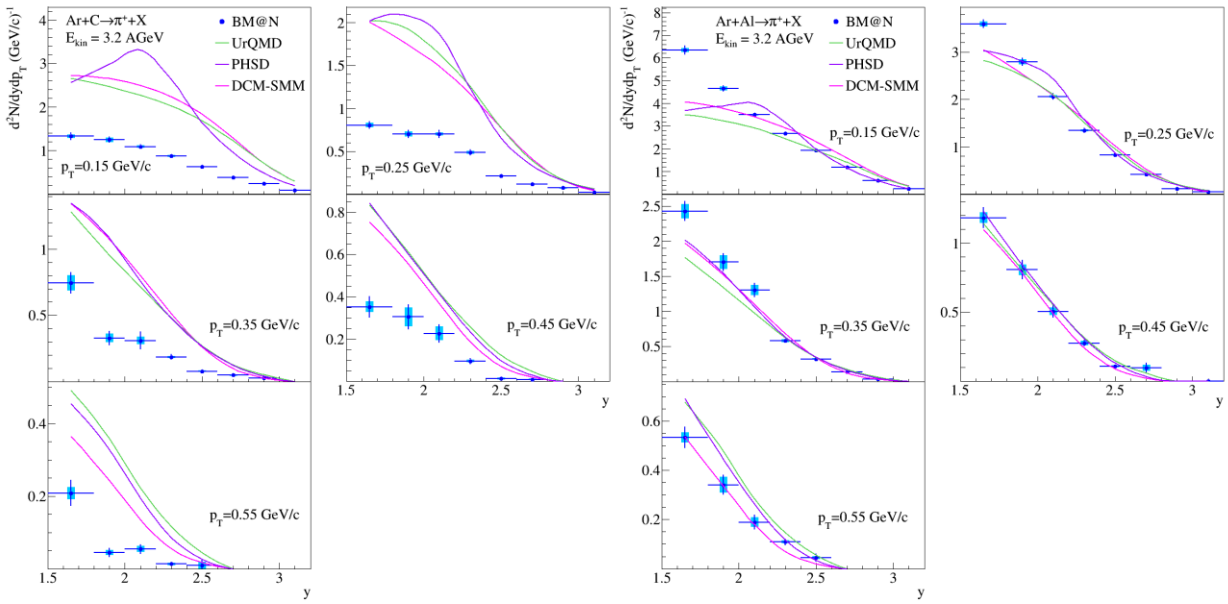

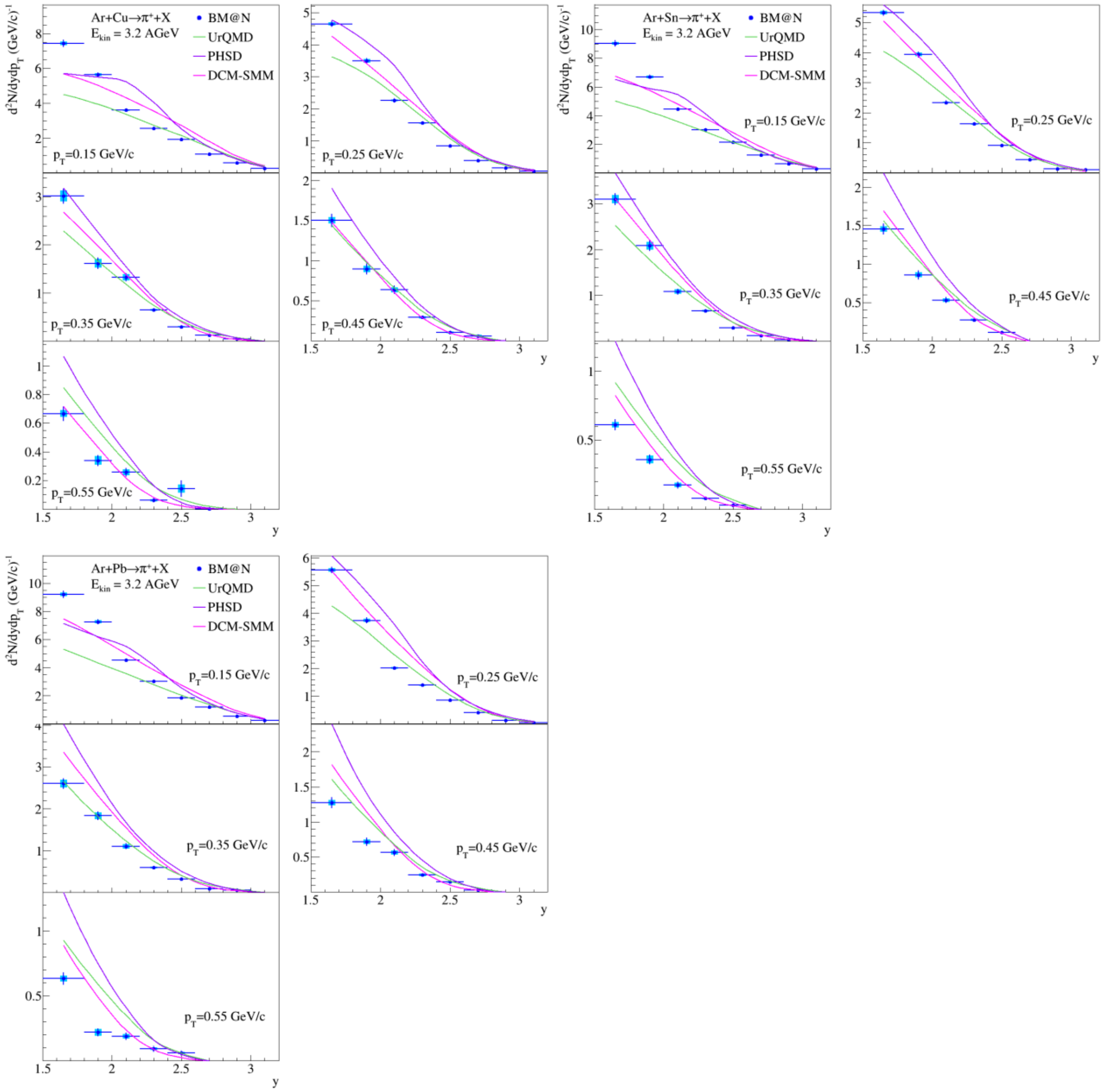

Fig. 15a. Reconstructed rapidity y spectra of π^+ measured in bins of p_T in minimum bias *Ar+C, Ar+Al, Ar+Cu*, *Ar+Sn, Ar+Pb* interactions at 3.2 AGeV argon beam energy. The error bars represent the statistical errors, the boxes show the systematic errors. Predictions of the DCM-SMM, UrQMD and PHSD models are shown as rose, green and magenta lines.

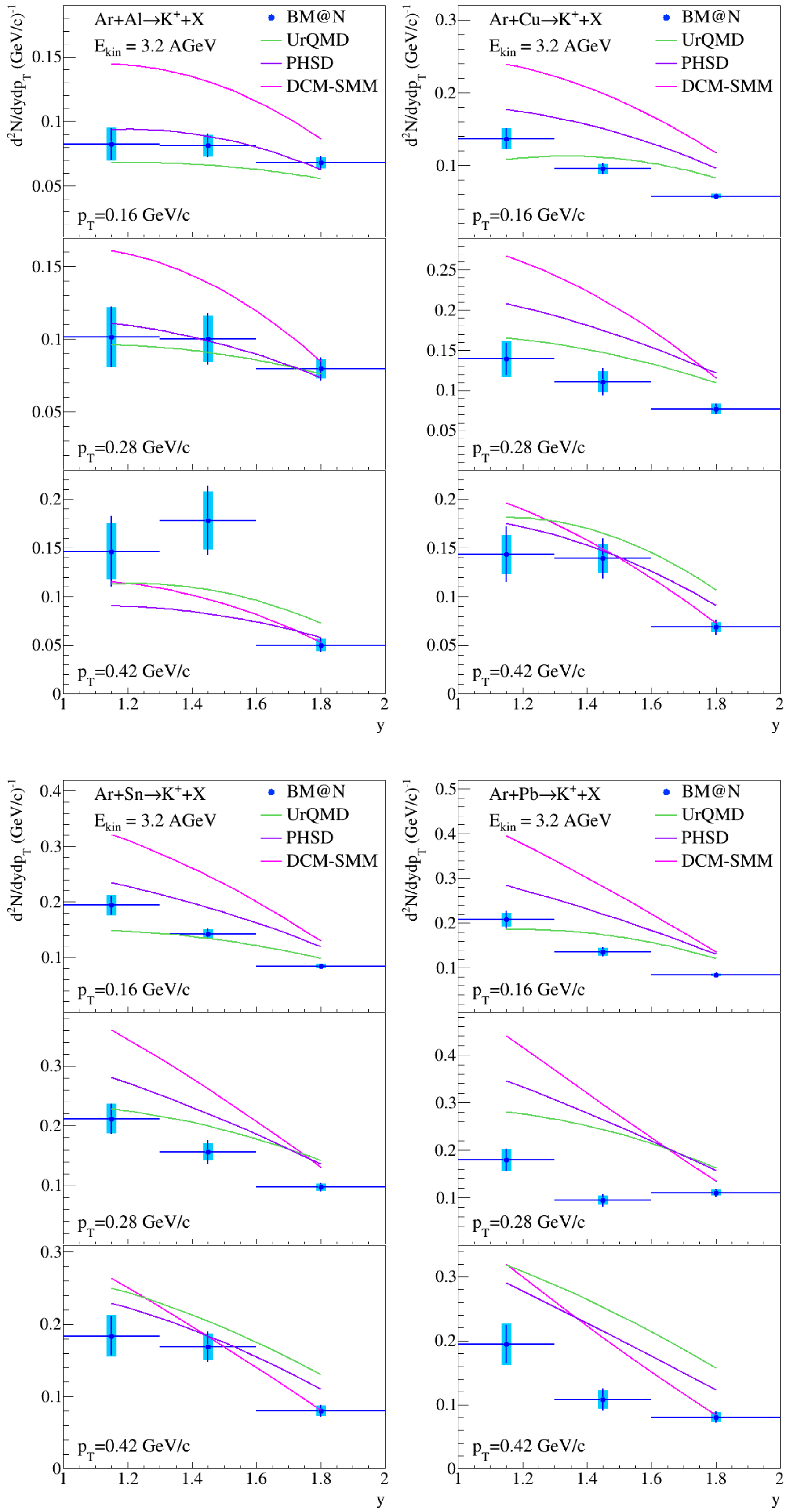

Fig. 15b. Reconstructed rapidity y spectra of K+ measured in bins of p_T in minimum bias Ar+Al, Ar+Cu, Ar+Sn, Ar+Pb interactions at 3.2 AGeV argon beam energy. The error bars represent the statistical errors, the boxes show the systematic errors. Predictions of the DCM-SMM, UrQMD and PHSD models are shown as rose, green and magenta lines.

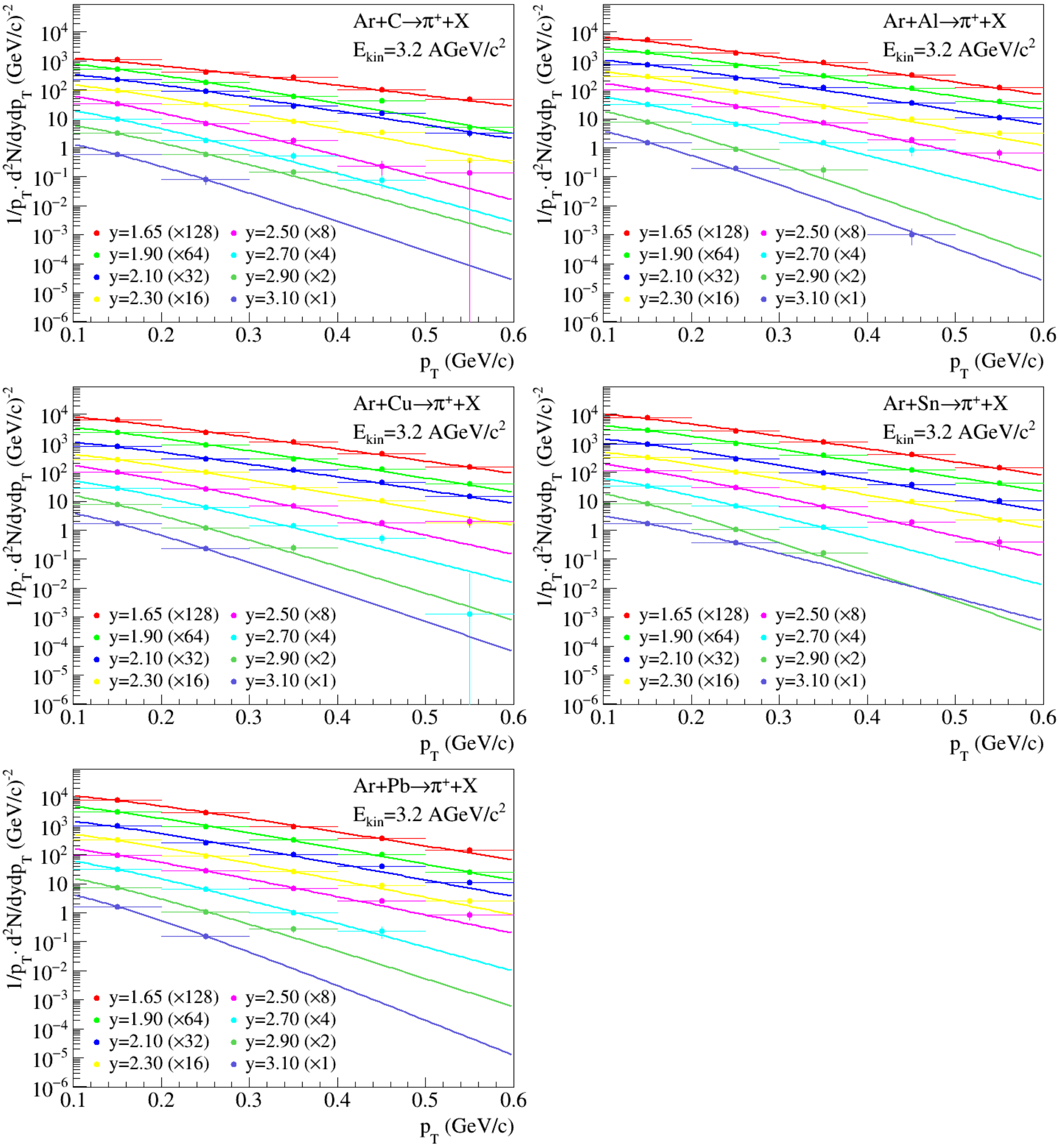

Fig.16a. Reconstructed invariant transverse momentum p_T spectra of π^+ measured in bins of rapidity in minimum bias *Ar+C*, *Ar+Al*, *Ar+Cu*, *Ar+Sn*, *Ar+Pb* interactions at 3.2 AGeV argon beam energy. Results of the fit described in the text are shown as colored lines.

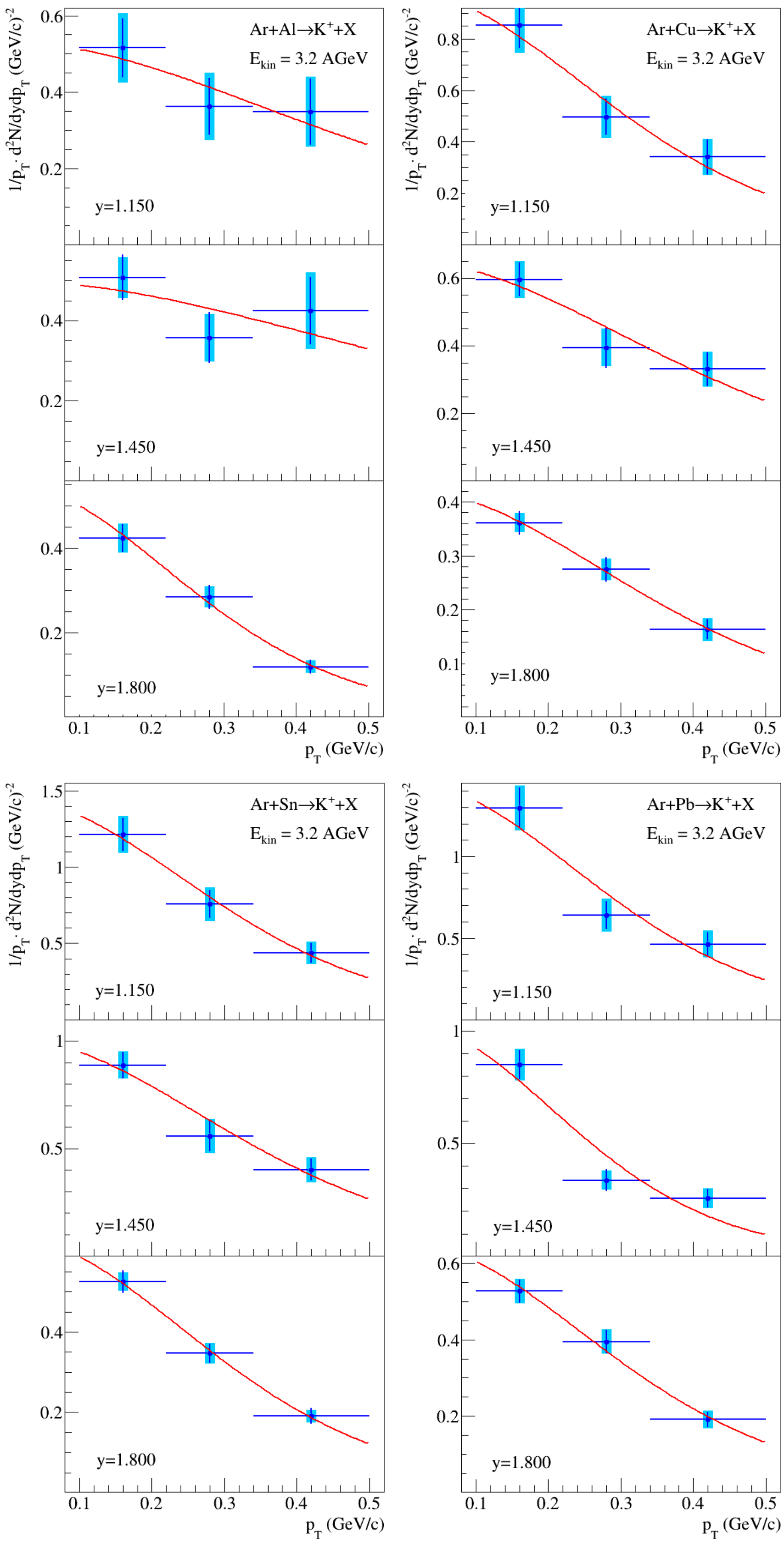

Fig.16b. Reconstructed invariant transverse momentum p_T spectra of K+ in minimum bias Ar+Al, Ar+Cu, Ar+Sn, Ar+Pb interactions at 3.2 AGeV argon beam energy. The error bars represent the statistical errors, the boxes show the systematic errors. Results of the fit described in the text are shown as lines.

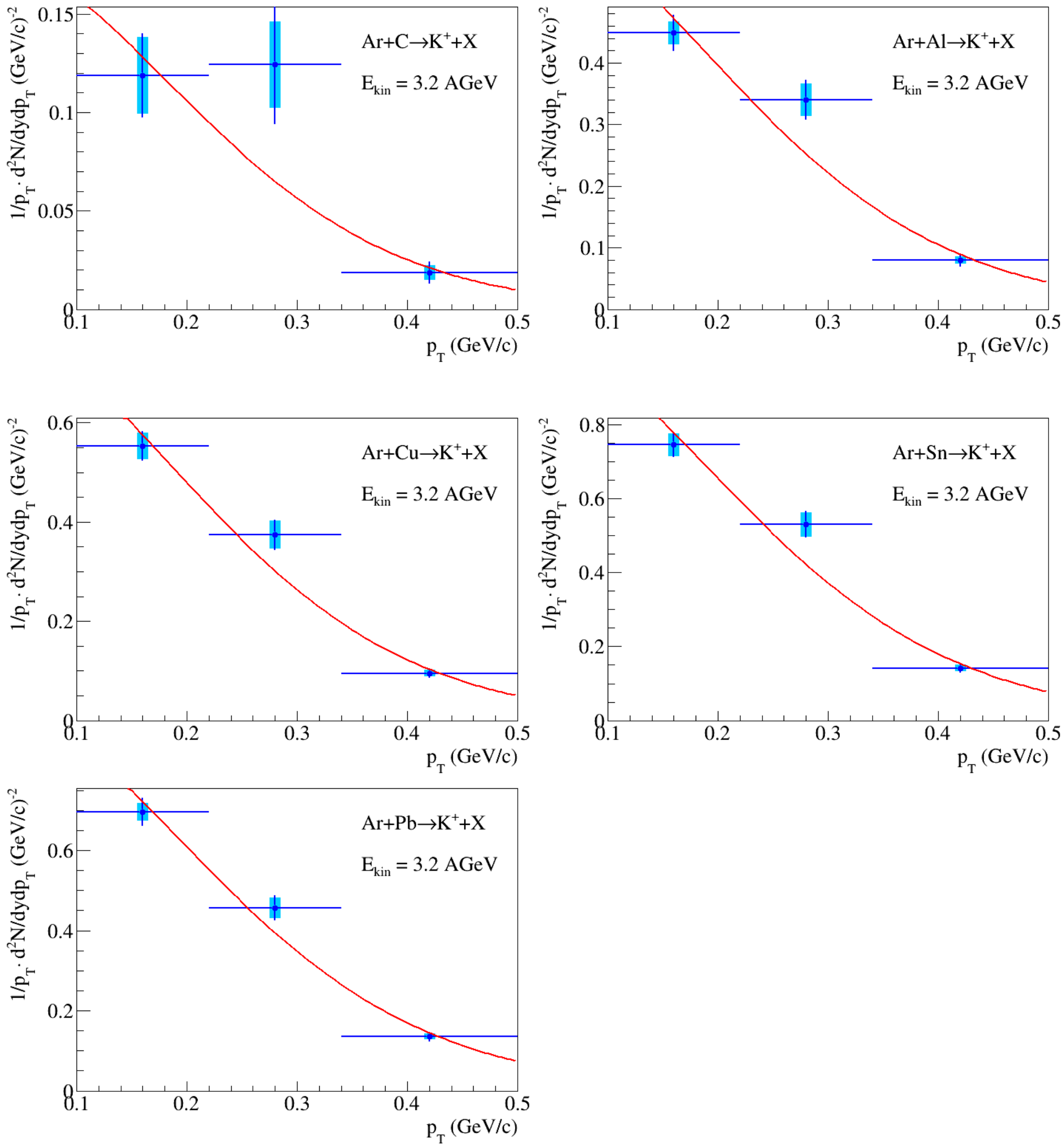

Fig.16c. Reconstructed invariant transverse momentum p_T spectra of K+ in the measured rapidity range in minimum bias A+C, Ar+Al, Ar+Cu, Ar+Sn, Ar+Pb interactions at 3.2 AGeV argon beam energy. The error bars represent the statistical errors, the boxes show the systematic errors. Results of the fit described in the text are shown as liness.

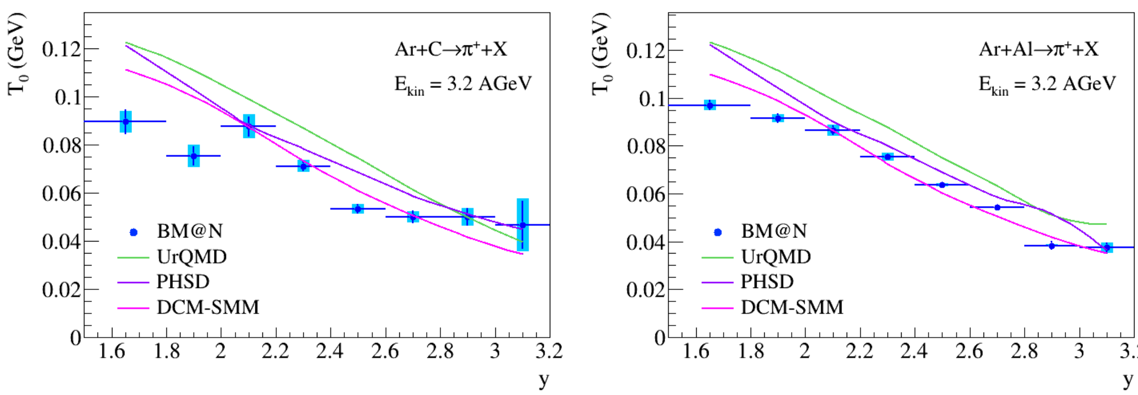

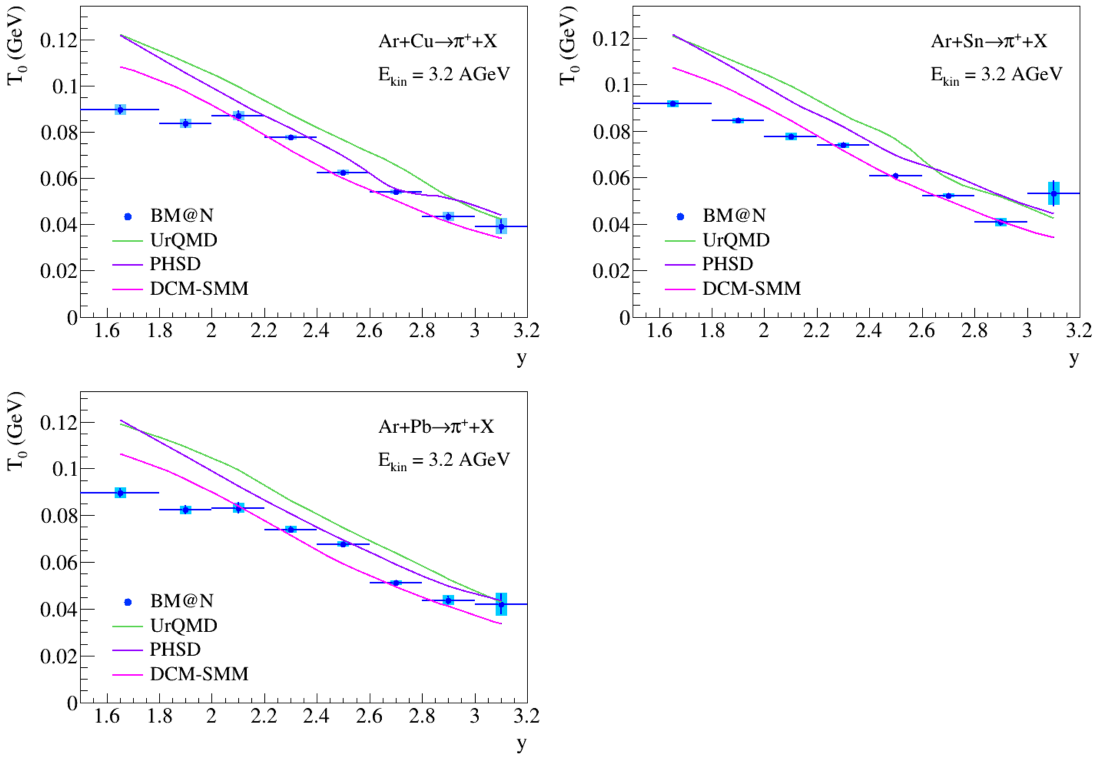

Fig17a. The y dependences of the inverse slope parameter T0 of the π+ invariant p_T spectra in *Ar+C, Ar+Al, Ar+Cu, Ar+Sn, Ar+Pb* minimum bias interactions. The error bars represent the statistical errors, the boxes show the systematic errors. Predictions of the DCM-SMM, UrQMD and PHSD models are shown as rose, green and magenta lines.

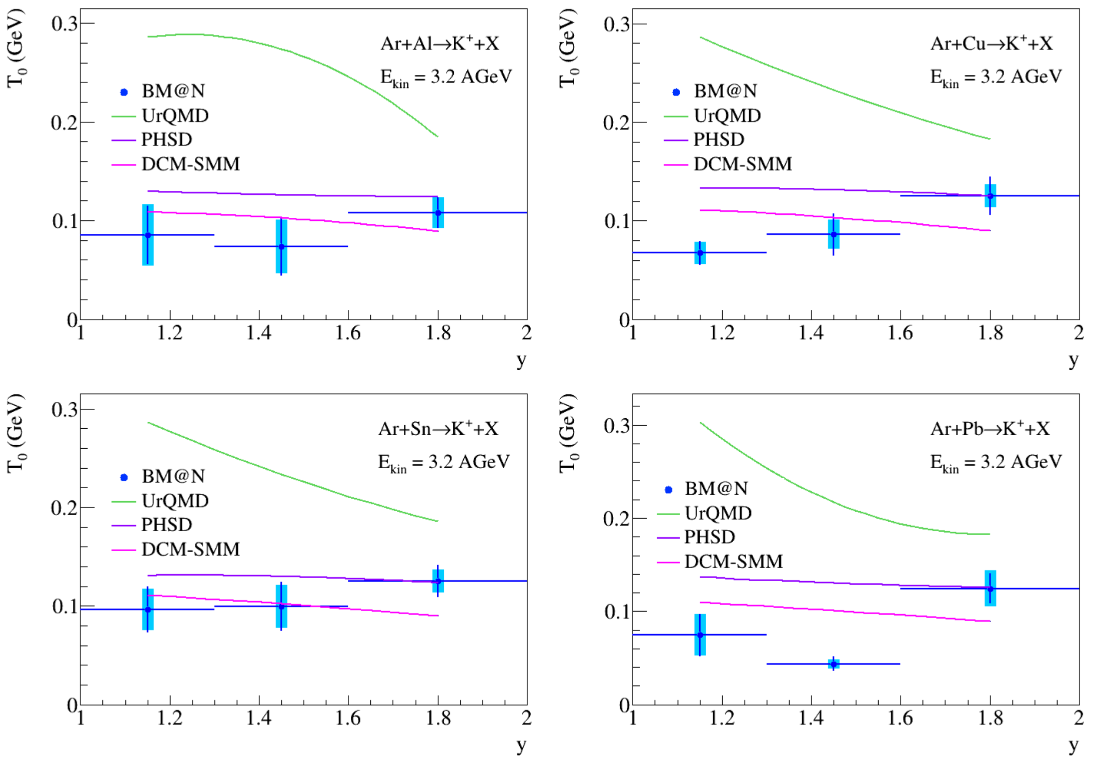

Fig17b. The y dependences of the inverse slope parameter T0 of the K+ invariant p_T spectra in Ar+Al, Ar+Cu, Ar+Sn, Ar+Pb minimum bias interactions. The error bars represent the statistical errors, the boxes show the systematic errors. Predictions of the DCM-SMM, UrQMD and PHSD models are shown as rose, green and magenta lines.